
Article

Not peer-reviewed version

Conceptual Design of a Low-cost Class-III turbofan based UCAV Loyal Wingman

[Savvas Roussos](#) , Eleftherios Karatzas , [Vassilis Kostopoulos](#) ^{*} , [Vaios Lappas](#)

Posted Date: 15 May 2025

doi: [10.20944/preprints202505.1151.v1](https://doi.org/10.20944/preprints202505.1151.v1)

Keywords: UCAV; loyal wingman; class-III UAV; conceptual design



Preprints.org is a free multidisciplinary platform providing preprint service that is dedicated to making early versions of research outputs permanently available and citable. Preprints posted at Preprints.org appear in Web of Science, Crossref, Google Scholar, Scilit, Europe PMC.

Copyright: This open access article is published under a Creative Commons CC BY 4.0 license, which permit the free download, distribution, and reuse, provided that the author and preprint are cited in any reuse.

Disclaimer/Publisher's Note: The statements, opinions, and data contained in all publications are solely those of the individual author(s) and contributor(s) and not of MDPI and/or the editor(s). MDPI and/or the editor(s) disclaim responsibility for any injury to people or property resulting from any ideas, methods, instructions, or products referred to in the content.

Article

Conceptual Design of a low-cost Class-III turbofan based UCAV Loyal Wingman

Savvas Roussos ^{1,†}, Eleftherios Karatzas ^{1,3}, Vasilis Kostopoulos ^{1,*} and Vaios Lappas ²

¹ Department of Mechanical Engineering & Aeronautics, University of Patras, Rion-Patras, University Campus, GR 26504

² Department of Aerospace Science & Technology, National & Kapodistrian University of Athens, Psahna Evias, 34400, Greece

³ Research, Technological Development and Innovation Center, Hellenic National Defense General Staff, Vari, Athens, 16672, Greece

* Correspondence: kostopoulos@upatras.gr

† Author to whom correspondence should be addressed.

Abstract: The rapid evolution of military technology has led to an increased interest in Unmanned Combat Aerial Vehicles (UCAVs). This research focuses on the conceptual design of a low-cost, turbofan-powered UCAV, specifically a Class-III aircraft as defined by NATO classification (STANAG 4670), with a target take-off weight of approximately one tonne. The study adopts a "from scratch" design approach, recognizing the limitations of existing data and the potential for scaling errors. This approach involves a meticulous design process that includes the development of precise requirements, weight estimations, and iterative optimization of the aircraft layout to ensure aerodynamic efficiency and operational functionality. A key element of this conceptual design is its focus on a low-cost profile, achieved through the adoption of a simplified structural layout, and the integration of off-the-shelf components where possible. The design process involves an iterative approach, beginning with fundamental requirements and progressing through the detailed development of individual components and their integration into a cohesive aircraft. The study details the selection of an existing and operational engine due to its power output. The design and analysis of the wing, fuselage, and V-tail configuration are presented, incorporating considerations for aerodynamic efficiency, stability, weight estimation, and internal component layout. The study concludes by outlining recommendations for future work, including high-fidelity CFD simulations, structural analysis, and the integration of advanced electronic systems and AI capabilities essential for the Loyal Wingman concept.

Keywords: UCAV; loyal wingman; class-III UAV; conceptual design

1. Introduction

1.1. Overview

The rapid evolution of military technology has spurred interest in Unmanned Combat Aerial Vehicles (UCAVs), which offer enhanced mission capabilities, reduced risk to human pilots, and greater operational flexibility. The "Loyal Wingman" concept, where UCAVs collaborate autonomously with manned aircraft, represents a key advancement in modern warfare, extending the reach of manned platforms in roles such as intelligence, surveillance, reconnaissance, electronic warfare, and offensive combat operations. Acting as force multipliers, these UCAVs provide operational versatility while mitigating risks to human pilots.

At the moment, Loyal Wingman UCAVs face design challenges due to the scarcity of verified empirical data and the infancy of the concept. Limited or inconsistent information makes accurate performance modeling and weight estimation difficult, particularly when scaling existing designs to larger, more complex UCAVs. To address this, the research adopts a "from scratch" design approach, focusing on a Class-III (NATO Classification, STANAG 4670 [1]) turbofan-based UCAV with a target takeoff weight of approximately one tonne, lighter than any existing developmental UCAV up to date. Existing UCAV designs are compared in terms of their performance characteristics and payload

capacity, as a foundation to extract the requirements for this design. This approach ensures an optimized and cost-effective design tailored to specific operational requirements, avoiding the pitfalls of scaling existing profiles. The study emphasizes affordability through simplified structural layouts, reliance on commonly-used manufacturing methods, and the integration of off-the-shelf components where possible, such as a standardized turbofan engine and materials.

It is based on the master's thesis titled "Conceptual Design of a Turbofan-Based Loyal Wingman UAV: Towards a Class-III Aircraft" by the contributing author Roussos [2], supervised by professors Lappas, Kostopoulos and co-supervised by PhD candidate Karatzas, and focuses on the design of the wing, tail, and internal layout and spatial planning for optimal weight distribution and center of gravity management. In-depth analyses of structural integrity, AI systems, flight controls, sensors, and detailed payload integration fall beyond the scope of this first study.

1.2. State Of The Art

The late 20th century saw breakthroughs in autonomous aircraft. Modern UAVs exemplify a convergence of advanced technologies, expanding their capabilities across military and civilian domains. Notable platforms like the RQ-2 "Pioneer" and MQ-1 "Predator" showcased UAVs' dual utility for surveillance and combat operations. The emergence of smaller, tactical UAVs such as the RQ-11 "Raven" and Black Hornet Nano reflected a growing demand for portable, easily deployable systems for ground forces. The integration of Artificial Intelligence (AI) further enhanced UAV autonomy, decision-making, and mission flexibility.

Today's UAVs perform a wide range of functions, from intelligence gathering and combat to logistical support. Class III UAVs, with their larger payload capacities and extended endurance, are particularly suited for the role of a Loyal Wingman. The "Tísis" UCAV exemplifies this concept, as a one-tonne, turbofan-powered Class III platform (NATO Classification) designed to collaborate with manned systems. Its design could reflect cutting-edge advancements and aim to demonstrate the feasibility of future unmanned combat systems. The historical trajectory and state-of-the-art developments in UAVs illustrate a dynamic field shaped by technological innovation and evolving mission requirements.

1.3. Existing UCAV Comparative Analysis

This section aims to identify the key requirements for the conceptual design of a Loyal Wingman UCAV by analyzing trends observed in existing and developmental jet-powered Class-III UCAVs (Table 1). The analysis evaluates performance parameters to establish clear design criteria essential for shaping the foundational parameters of a 1-tonne UCAV, ensuring it aligns with the characteristics of a Loyal Wingman while remaining competitive and operationally viable in real-world scenarios.

Most existing UCAVs fit the profile of intelligence, surveillance, reconnaissance (ISR), and precision strike platforms due to their design characteristics and operational roles. Models like the S-70 Okhotnik-B and nEUROn prioritize stealth, endurance, and long-range capabilities over agility and maneuverability, making them less aligned with the traditional "dogfighter" profile, which demands high agility and exceptional maneuverability. Among current designs, the Kizilelma-A stands out with its emphasis on high-speed, maneuverability, and a larger payload capacity, suggesting potential for closer engagement profiles. However, the UCAV designed in this thesis will follow multi-role "Loyal Wingman" trends, incorporating agility and versatility without focusing specifically on dogfighting.

Table 1. Specifications of existing developmental UCAV models.

Model	Configuration	MTOW [lb]	Empty Weight [lb]	Max. Speed [kts]	Payload [lb]	Percentage of MTOW	Length- to- wingspan Ratio
Anka-III [3]	Flying Wing	14330	-	425-450	1653	11.5%	1.22
CATS Warrior [4]	Conventional	4630	-	Mach 0.9	-	-	
Kizilelma-A [5]	Canard	13200	-	590	3300	25%	1.51
MQ-28 Ghost Bat [6-8]	Conventional	-	-	600	-	-	1.60
nEUROn [9]	Flying Wing	15432	10803	529	1014	6.6%	0.76
S-70 Okhotnik-B [10-12]	Flying Wing	55116	-	540	4410-6172*	8.0-11.2%	0.79
X-45A [13,14]	Hybrid	-	8000	533	-	-	0.78
XQ-58 Valkyrie [16-18]	Conventional	6000	2500	566	1200	20%	1.20

* Not Confirmed.

1.4. Design Uniqueness and Novelty

The novelty of this UCAV design resides mainly in the concept itself. Potentially establishing a new weight category with a Maximum Takeoff Weight (MTOW) of 1000 kg—approximately half that of the lightest current developmental model (e.g., HAL CATS Warrior, maiden flight planned for 2025)—this lightweight configuration, combined with high-speed capability and a high percentage of MTOW allocated to payload, enables mission-specific flexibility through trade-offs between payload and fuel to extend range or boost speed, hence the importance of achieving a high percentage of MTOW utilized for payload as will be examined in the upcoming sections of this article. The compact size allows for operations from minimal runways or static rocket-assisted launches, while inherently contributing to a reduced radar cross-section. As the first UCAV conceived from scratch in Greece, tailored to cover the country's operational range and collaborate with aircraft operated by the Hellenic Air Force, this design represents a significant step in lightweight Loyal Wingman development.

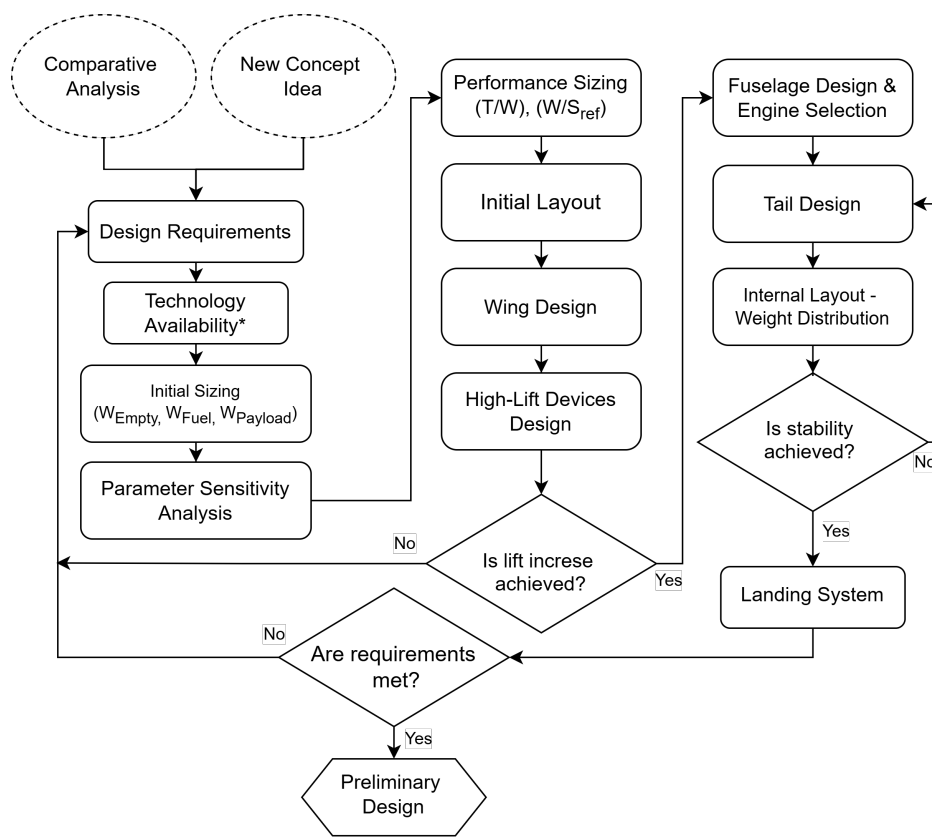


Figure 1. Flow chart of the conceptual design process followed in this study

2. Methodology and Design Process

2.1. Conceptual Design Methodology

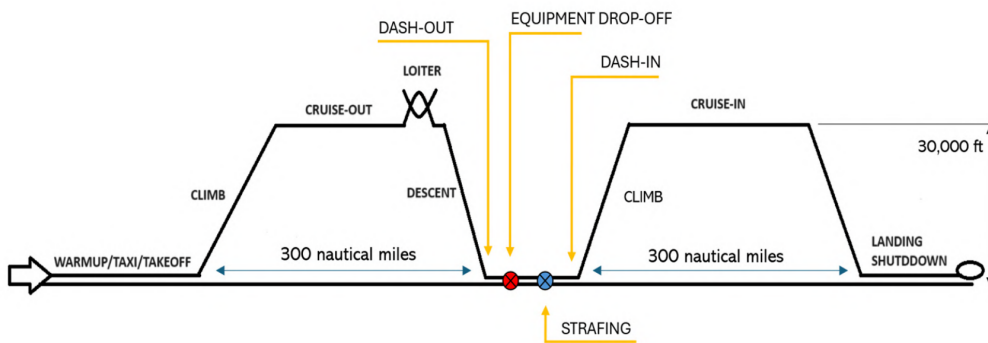
The design methodology followed for this design (Figure 1) is a farrago of well-established approaches for designing an aircraft, from designers such as I. Roskam, D. Raymer and M. Sadraey [19–21], whose methodologies have been thoroughly followed in this study. Roskam's methods were utilized for initial and performance sizing, providing most empirical values for parameters such as L/D and SFC. Raymer's work complemented Roskam's, particularly regarding aspect ratio, SFC variation, and correlations between empty weight and MTOW for similar manned aircraft and UAVs. Sadraey contributed to the methodology for wing, tail, and fuselage design, static stability analysis, weight estimation of various components, and landing system design, especially the critical angles for ground stability. Finally, Kallinteris [22] provided additional empirical data and restrictions for these critical angles during landing system design, along with design considerations about HLD design and the estimation of available fuel space inside the wings.

2.2. Design Requirements

The mission requirements for the "Tísis" UCAV prioritize a balance between performance and feasibility, guided by benchmarks from operational UCAVs like the ones mentioned in Table 1. While larger platforms achieve greater ranges and speeds, the design constraints of a 1-tonne UCAV necessitate trade-offs in altitude, endurance, and propulsion. Key parameters—such as ambient conditions ($T_{\text{ambient}} = 25^{\circ}\text{C}$ at sea level), takeoff/landing distances, high-speed—are tailored to align with Hellenic Air Force operational needs, though they remain ambitious given the platform's smaller size. The flight profile (Figure 2) and detailed specifications (Table 2) reflect these calibrated goals. It should be noted that, although total endurance is not prioritized, a loitering capability of 20 minutes is specified to support mission adaptability.

Table 2. Initial Design Requirements for the "Tísis" UCAV.

Parameter	Target Quantity	Note
Gross Weight	1000 kg \pm 10%	Initial Requirement
Empty Weight	-	To Be Determined
Dash Ceiling	5000 ft	-
Cruise Ceiling	30000 ft	-
Dash Speed	Mach 0.90	At Dashing Altitude
Cruise Speed	Mach 0.80	At Service Altitude
Range	300 Nautical Miles	-
Loitering Endurance	20 minutes	-
Payload Weight	>20%	Percentage of MTOW
Take-off Groundrun Distance	\leq 1000 ft	MIL-STD-3013A
Total Landing Distance	\leq 1000 ft	MIL-STD-3013A
Climb Duration	10 minutes	Clean Configuration
Engine Type	Turbofan	-

**Figure 2.** The scheme of the UCAV's mission profile.

2.3. Initial Sizing

2.3.1. Iterative Refinement of Weight Estimations

The initial sizing of the "Tísis" UCAV employs an iterative method to estimate empty weight, fuel requirements, and payload capacity. Due to the limited availability of data on Class-III UAVs, empirical data from manned subsonic and transonic military aircraft are used and adjusted to account for modern aerodynamic and propulsion advancements. Parameters such as specific fuel consumption (c_j) and maximum lift-to-drag ratio (L/D)_{max} are obtained from literature and refined through aerodynamic simulations [20].

The iterative process starts with an assumed payload fraction of MTOW, from which empty and fuel weights are computed. Empty weight estimation follows a logarithmic correlation with MTOW, and fuel weight is determined using mission-specific performance models, notably the Breguet range equation for cruise and loiter. A reserve fuel margin of 5% MTOW and a trapped fuel allocation of 0.5% are included. The process converges once the calculated empty weight meets a predefined error threshold. Key design inputs include:

- A wing aspect ratio derived from statistical data for conventional configuration.
- Modified, thrust-specific fuel consumption values for a low-bypass ratio (LBR) turbofan engine without afterburner.

All parameters and fuel ratios f for each mission phase are summarized in Table 3.

Table 3. Considered quantities for the initial sizing in all mission phases

<i>i.</i>	Mission Phase	SFC_i (lbs/hr/lbf)	$(L/D)_{max_i}$	Fuel Ratio f_i
1	Engine Warm-up	-	-	0.99
2	Taxiing	-	-	0.99
3	Take-off	-	-	0.99
4	Climb	-	-	0.97
5	Cruise-out	0.7392	5.50	0.952
6	Loiter	0.7000	9.00	0.9619
7*	Descend-1	-	-	1.00
8*	Dash-out	0.8000	5.50	0.9884
9	Drop-off	-	-	1.00
10	Strafing	0.9000	4.00	0.9814
11	Dash-in	0.8000	5.50	0.9884
12	Climb	-	-	0.97
13	Cruise-in	0.7392	5.50	0.9511
14	Descend-2	-	-	0.9925
15	Landing & Engine Switch-off	-	-	0.995

* Phases 7 and 8 are combined for the design process.

2.3.2. Streamlined Methodology

To reduce design time and development costs, the methodology prioritizes pragmatic decisions over highly detailed conceptual estimation. Reference data from manned subsonic and transonic military jets forms the foundation for initial configuration definition. Raymer's method [20], linking $(L/D)_{max}$ to wetted aspect ratio ($AR_{wet} = AR \cdot S_{ref} / S_{wet}$), is selectively employed and refined using empirical corrections for improved aerodynamic fidelity. The sizing process is conducted for three MTOW values—900 kg, 1000 kg, and 1100 kg—to evaluate payload efficiency. As shown in Table 4, the 1100 kg case yields the most favorable payload-to-MTOW ratio and is therefore selected as the final design reference.

2.3.3. Challenges and Limitations

Designing a Loyal Wingman UCAV poses unique challenges, primarily due to the developmental nature of such systems and the scarcity of direct empirical data. While leveraging data from comparable manned aircraft accelerates early-stage design, it introduces uncertainties, particularly in fuel and weight estimations. These limitations are addressed through a sensitivity analysis that quantifies how variations in key assumptions—such as payload fraction, fuel consumption, and aerodynamic efficiency—affect MTOW. The findings, provided in Table 5, guide refinement priorities and ensure robustness in weight budgeting.

Table 4. Initial sizing results for 3 cases of MTOW

	Run 1		Run 2		Run 3	
	[lb]	[kg]	[lb]	[kg]	[lb]	[kg]
W_{TO}	1984.16	900.00	2204.62	1000.00	2425.09	1100.00
W_{Empty}	989.02	448.61	1084.36	491.86	1178.49	534.55
W_{Fuel}	589.80	267.53	655.34	297.26	720.87	326.98
$W_{Payload}$	402.39	182.52	461.65	209.4	522.12	236.83
$W_{Payload}/W_{TO}$	20.28%		20.94%		21.53%	

Table 5. Concentrated results of the parameter sensitivity analysis

Parameter	Breguet Partials (lbs/unit)	
	Range Case	Endurance Case
Range R [nautical miles]	Cruise-out	+2.7011
	Cruise-in	+2.7011
	Dash-out	+3.2150
	Dash-in	+3.2150
Endurance E [hours]	Loitering	– +1067.76
Specific Fuel Consumption c_i [lb/lbf/hr]	Cruise-out	+913.55
	Cruise-in	+931.82
	Dash-out	+209.60
	Dash-in	+209.60
	Loitering	– +762.69
(L/D)	Cruise-out	–86.57
	Cruise-in	–88.31
	Dash-out	–29.23
	Dash-in	–29.23
	Loitering	– –59.32

2.4. Configuration Selection and Rationale

A conventional configuration with a wing and aft tail was selected for the UCAV based on practical, operational, and developmental criteria, as well as reference to aircraft such as the XQ-58 Valkyrie and MQ-28 Ghost Bat. This layout is well-documented, supports predictable stability and control characteristics, and facilitates efficient design within the project's limited 6–8 month timeframe [20]. The mission profile—emphasizing strafing and agile maneuvers in mid- to high-subsonic regimes—requires handling qualities best provided by conventional configurations.

Alternative layouts such as delta-wings or flying-wings were considered but dismissed. Delta wings, although structurally efficient and favorable for high-speed flight, suffer from poor low-speed handling and pitch stability issues. Flying-wing designs offer stealth and endurance advantages but lack agility and require advanced fly-by-wire systems for stability [23]. The selected configuration achieves a balanced compromise between maneuverability, simplicity, and cost-effectiveness, aligning with the design objectives for a reliable, low-cost Loyal Wingman UCAV.

2.5. Performance Sizing

This stage of the design process serves the purpose of determining the minimum reference area for the main lifting surfaces (S_{ref}) of the aircraft and the minimum required thrust (T). The performance sizing is conducted based on the four following performance criteria:

- Takeoff Distance
- Landing Distance
- Flight Speed
- Climbing Performance

These criteria are based on regulations, such as FAR-23 for propeller airplanes, FAR-25 for jet-powered aircraft and MIL-3013A for military aircraft. Their application is performed according to the methodology by I. Roskam [19] and utilized in this study, from which all the equations and application methods presented below are taken.

The determination of the total drag coefficient (C_D) is a critical step in the conceptual design phase of the "Tísis" UCAV, since it directly influences the aircraft's performance characteristics. C_D comprises two primary components: zero-lift or parasitic drag (C_{D0}) and induced drag ($k \cdot C_L^2$), for use in performance sizing calculations.

$$C_D = C_{D0} + k \cdot C_L^2 \quad (1)$$

where k is the induced drag term, which is further defined as $k = 1/(\pi \cdot AR \cdot e)$ where AR is the wing aspect ratio, and e is Oswald's efficiency coefficient. Empirical data from existing comparable aircraft were utilized to estimate C_{D_0} . First, an indicative value for $(W/S_{ref})_{TO}$ at 50 psf is chosen. This value may be subjected to reevaluation in later stages of the design process. Since the MTOW is known, this assumption yields a tentative wing reference area of 48.5 ft². The relationship used to estimate the parasitic drag for the aircraft is presented in Equation (2) [20,22].

$$C_{D_0} = \bar{C}_f \frac{S_{wet}}{S_{ref}} \quad (2)$$

where S_{ref} is the wing reference area, S_{wet} the total wetted area of the UCAV and \bar{C}_f is a mean friction coefficient, which is assumed to be 0.0035 for fighter aircraft [20]. The total wetted surface can be tentatively estimated based on empirical data through the utilization of Equation (3).

$$S_{wet} = 10^c \cdot W_{TO}^d \quad (3)$$

where c, d equal -0.1289 and 0.7506, respectively [22]. The resulting wetted area is 258.03 ft² yielding a parasitic drag coefficient of 0.01862 via Equation (2).

Increments to C_{D_0} are applied for high-lift devices (HLD), landing gear, and compressibility effects during high-speed flight, as detailed in Tables 6 and 7. External components (e.g., sensors, antennas) and interference drag (5%–10% of total drag) are acknowledged but not explicitly quantified. No additional ΔC_{D_0} is considered for interference drag due to the engine's internal placement and proper design practices.

Table 6. Standard values of the increase in parasite drag coefficient and the change in Oswald's coefficient with deployed HLD and landing gear [22]

Layout	ΔC_{D_0}	Oswald's Coefficient e
Clean Flight	0.0	0.85
HLD - Take-Off Configuration	0.010–0.020	0.80
HLD - Landing Configuration	0.055–0.075	0.75
Landing Gear Deployed	0.015–0.025	No effect

Table 7. Estimated increase in parasitic drag coefficient due to compressibility [22]

Flight Speed (knots)	Altitude (feet)	ΔC_{D_0}
481.65 (Mach 0.80)	30000	0.0010
595.42 (Mach 0.90)	5000	0.0025

The wing aspect ratio (AR) is initially derived from D. Raymer's method for canard-bearing aircraft, which accounts for the additional lift provided by canards and the conceptual sketch-based method mentioned in Subsection 2.3.2, adjusted by a factor of 0.9 to account for the absence of a canard on "Tísis" UCAV. The final AR of 5.0 is selected, with drag polars calculated and presented in Table 8. Maximum lift coefficients for take-off ($C_{Lmax,TO}$) and landing ($C_{Lmax,L}$) are tentatively set to 2.0 and 2.4, respectively, based on [19,22]. Air density values are obtained from Table A1.

Table 8. Drag Polars and Oswald's coefficient for all flight phases of interest

Phase	Oswald's Coefficient e	Drag Polars	
		C_{D_0}	$k \cdot C_L^2$
Take-Off	0.80	0.0536	$0.0796 \cdot C_L^2$
Landing	0.75	0.0686	$0.0849 \cdot C_L^2$
Cruise	0.85	0.0196	$0.0749 \cdot C_L^2$
Dash	0.85	0.0211	$0.0749 \cdot C_L^2$

2.5.1. Performance Criterion [1]: Takeoff Field Distance

The take-off field length (S_{TOFL}) includes the ground run distance (S_{TOG}), with a requirement of $S_{TOG} \leq 1000$ ft. The relationship between thrust-to-weight ratio (T/W) and weight-to-wing reference area ratio (W/S_{ref}) is given by the empirical formula in Equation (4).

$$S_{TOG} = \frac{0.0447 \cdot (W/S_{ref})_{TO}}{\rho \cdot \left(C_{Lmax_{TO}} \cdot \left[\frac{0.75 \cdot (5 + \lambda_e)}{(4 + \lambda_e)} (T/W)_{TO} - \mu_G \right] - 0.72 \cdot C_{D_0} \right)} \leq 1000 \text{ ft} \quad (4)$$

where ρ is air density, $\lambda_e = 3.0$ is the assumed bypass ratio for an LBR turbofan engine and $\mu_G = 0.025$ is the friction coefficient for a dry tarmac runway [21,34]. The relationship between (T/W) and (W/S_{ref}) according to this criterion is the following:

$$(W/S_{ref})_{TO} = 88.10 \cdot (T/W)_{TO} - 2.5696 - 0.0887 \quad (5)$$

2.5.2. Performance Criterion [2]: Landing Field Distance

The landing distance criterion follows military specifications (MIL-STD-3013A), similar to FAR-25 regulations, with the key difference being that the approach speed for military aircraft is generally a smaller proportion of their stall speed than that of commercial airplanes. A maximum landing distance S_L of 1000 ft is required initially (Table 2). A conservative approach is applied, assuming:

1. No payload is discarded.
2. Fuel consumption is less than the total mission requirement.
3. No thrust degradation occurs (takeoff and landing altitudes match).
4. The UCAV is assumed to weigh 85% of its MTOW during approach to account for this conservative scenario.

The landing field distance criterion is based on approximations of the approach speed (V_A) and the stall speed in landing configuration ($V_{Stall,L}$):

$$V_A = \sqrt{\frac{S_{FL}}{0.3}} = \sqrt{\frac{S_L}{0.3 \cdot 0.6}} = 74.54 \text{ kts} \quad (6)$$

$$V_{Stall,L} = \sqrt{\frac{2 \cdot (W/S_{ref})_L}{\rho \cdot C_{Lmax_L}}} = \frac{V_A}{1.2} \quad (7)$$

This relationship between V_A and $V_{Stall,L}$ is dictated by military standards. By translating V_A from knots to fps and considering the assumed maximum lift coefficient in landing configuration of 2.4, the criterion yields the following relationship:

$$(W/S_{ref})_{TO} \leq 35.64 \text{ psf} \quad (8)$$

2.5.3. Performance Criterion [3]: Flight Speed

The analysis targets two key high-speed flight conditions: cruise and dash. For steady, level flight, the equations governing thrust (T) and lift (L) are given by:

$$T = D = \frac{1}{2} \rho \cdot V^2 \cdot C_D \cdot S_{\text{ref}}, \quad (9)$$

$$L = W = \frac{1}{2} \rho \cdot V^2 \cdot C_L \cdot S_{\text{ref}}, \quad (10)$$

D being the aerodynamic drag, W the aircraft's weight, V the flight speed and ρ the air density at flight altitude. By combining the last two equations and substituting Equation (1) where needed, the thrust-to-weight ratio (T/W) can be expressed as a function of wing loading (W/S_{ref}):

$$\left(\frac{T}{W} \right)_i = \frac{C_{D_0} \cdot q}{(W/S_{\text{ref}})_i} + \frac{(W/S_{\text{ref}})_i}{\pi \cdot AR \cdot e \cdot q} \quad (11)$$

where $q = \frac{1}{2} \rho V^2$ is the dynamic pressure and i denotes the flight phase (e.g., cruise-out or dash-out).

Cruise-Out Phase

The UCAV is designed to maintain a cruise speed of Mach 0.80 at an altitude of 30000 ft. For this phase:

- The maximum cruise speed is assumed to be 1.2 times the specified cruise speed, resulting in $V_{\text{max, cruise}} = 577.98$ knots due to the fact that cruise speeds for jet aircraft are usually calculated at 75–80% thrust [21].
- The corresponding dynamic pressure is calculated as $q = 424.33$ psf.
- A conservative weight assumption is applied, using the maximum weight at the start of the cruise-out phase.
- A thrust lapse ratio adjusts the thrust-to-weight ratio for altitude-induced thrust degradation [21]:

$$T_{\text{altitude}} = T_{\text{sealevel}} \left(\frac{\rho_{\text{altitude}}}{\rho_0} \right) = T_{\text{sealevel}} \cdot \sigma \quad (12)$$

The relationship between (T/W) and (W/S_{ref}) adjusted to take-off weight and the altitude-induced thrust degradation at cruising altitude is the following:

$$\left(\frac{T}{W} \right)_{1,\text{TO}} = \frac{22.23}{(W/S_{\text{ref}})_{1,\text{TO}}} + \frac{(W/S_{\text{ref}})_{1,\text{TO}}}{2395.39} \quad (13)$$

Dash-Out Phase

The UCAV is required to reach a dash speed of Mach 0.90 at 5000 ft. For this phase:

- The dynamic pressure is calculated as $q = 1004.65$ psf.
- A conservative weight assumption is applied at the beginning of the dash-out phase.
- Thrust degradation is again considered using Equation (12).

Again, the relationship between (T/W) and (W/S_{ref}) adjusted to take-off weight and the altitude-induced thrust degradation at dashing altitude is the following:

$$\left(\frac{T}{W} \right)_{2,\text{TO}} = \frac{24.613}{(W/S_{\text{ref}})_{2,\text{TO}}} + \frac{(W/S_{\text{ref}})_{2,\text{TO}}}{15568.40} \quad (14)$$

2.5.4. Performance Criterion [4]: Rate of Climb (ROC)

The UCAV must meet specific ROC requirements as defined by military standards. These requirements are critical for ensuring the aircraft can achieve and sustain desired altitudes under various operational conditions [19]. Key altitude thresholds include:

- **Absolute ceiling:** The maximum altitude where the ROC reduces to zero.
- **Service ceiling:** The altitude where a ROC of 100 ft/min can be sustained.
- **Cruise ceiling:** The altitude where a ROC of 300 ft/min is maintained, typical for subsonic fighters.
- **Combat ceiling:** The altitude where a minimum ROC of 500 ft/min is achieved.

A linear relationship between ROC and altitude is assumed. Whether this relationship is linear in reality depends on the engine, the characteristics of the airplane, and the flight speed at which the climb is performed. Be that as it may, this assumption can be made and provide adequate results for the initial sizing [19].

The thrust-to-weight ratio (T/W) for ROC performance is derived from:

$$\left(\frac{T}{W}\right)_{ROC} = \frac{ROC}{\sqrt{\frac{2(W/S_{ref})}{\rho}} \sqrt{\frac{k}{C_{D_0}}}} + \frac{1}{(L/D)_{max}} \quad (15)$$

The lift-to-drag ratio is maximized for the optimum ROC and is calculated using the following formula:

$$(L/D)_{max} = \frac{1}{2} \sqrt{\frac{\pi \cdot AR \cdot e}{C_{D_0}}} \quad (16)$$

ROC – Cruising Altitude

At the cruise altitude of 30000 ft, the UCAV must maintain a minimum ROC of 300 ft/min, as stipulated by military standards [19,34]. Thrust is adjusted for altitude-induced degradation using $\sigma = 0.388$, and the weight is set to $W_c = 0.90 \cdot W_{TO}$, representing the mean cruise-out weight. Using aerodynamic data from Table 8 and air density values from Table A1, the relationship between (T/W) and (W/S_{ref}) is:

$$(T/W)_{TO} = \frac{11.6}{30.0807 \sqrt{(W/S_{ref})_{TO}}} + 0.1778 \quad (17)$$

ROC – Sea Level

Unlike the climb rate at cruise ceiling, which is specifically required, the sea level climb rate needs to be determined based on assumptions regarding the UCAV's performance. The sea level ROC is determined based on a linear ROC-altitude relationship, which is a reasonable assumption for initial sizing [19]. The UCAV is required to reach the cruise altitude of 30000 ft in 10 minutes (t_{climb}). An absolute ceiling (h_{abs}) is assumed. The ROC at a given altitude h and at sea level can be obtained from the following equations:

$$ROC_h = ROC_{sea_level} \left(1 - \frac{h}{h_{abs}} \right) \quad (18)$$

$$ROC_{sea_level} = \frac{h_{abs}}{t_{climb}} \cdot \ln \left(1 - \frac{h}{h_{abs}} \right)^{-1} = 7276.22 \text{ fpm or } 121.27 \text{ fps} \quad (19)$$

Fighter jets typically have steeper flight path angles during climb ($\gamma > 15^\circ$). For steep flight path angles the following applies:

$$ROC = V \cdot \sin \gamma \quad (20)$$

The design is based on the extreme scenarios; therefore, it will be assumed that the ROC is maximized, which requires maximizing the lift-to-drag ratio. Another assumption is made; at the beginning of

the climb phase the aircraft is in take-off configuration with retracted landing gear. By applying the methods of Roskam, [19], the relationship between (T/W) and (W/S_{ref}) is the following:

$$\frac{1}{\sqrt{(W/S_{ref})_{TO}}} = 0.3018 \cdot \left[0.9894 \left(\frac{T}{W} \right)_{TO} - \sqrt{-0.0105 \left(\frac{T}{W} \right)_{TO}^2 - 0.0106} \right] \quad (21)$$

2.5.5. Prevailing Performance Criterion

Each of the aforementioned criteria defines a constraint on the $(W/S_{ref})_{TO} - (T/W)_{TO}$ relationship, visualized in performance sizing graphs. These constraints, derived from Equations (5), (8), (13), (14), (17), and (21), create permissible design regions. The intersection of these regions defines the feasible design space, with the optimal solution expected along the boundary where the most restrictive constraints meet.

Initially, the landing field distance criterion determines the wing reference area (S_{ref}), while the dash speed criterion governs the minimum required thrust. After updating S_{ref} , the parasitic drag coefficient (Equation (2)) is recalculated, shifting the governing constraint to the sea-level ROC criterion for thrust. The final values are 1483.95 lbf for thrust and 68.04 ft^2 minimum wing reference area, as shown in Figure 3 and Table 9, respectively.

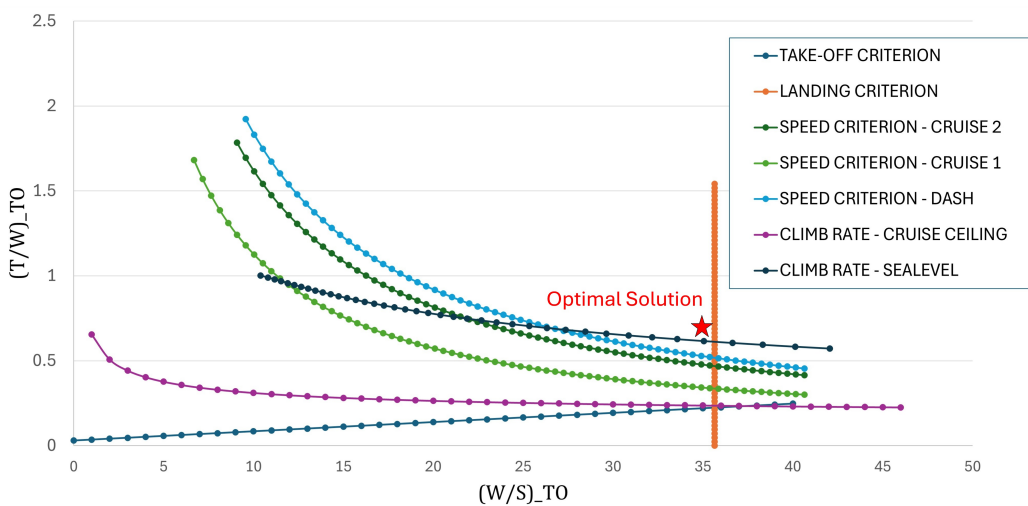


Figure 3. Acceptable values of (W/S) and (T/W) ratios and the optimal solution for the UCAV

Table 9. Minimum required wing reference area and engine thrust along with the prevailing (T/W) and (W/S_{ref}) ratios.

Iteration	(T/W)	(W/S_{ref})		$(T_{required})_{min}$ [lbf]	$(S_{ref_required})_{min}$ [ft^2]
		Input	Calculated		
#1	0.6928	50.0000	35.6428	1680.22	68.04
#2	0.6119	35.6428	35.6428	1483.95	68.04

2.6. Engine Selection

The engine selection process evaluated multiple low-bypass ratio (LBR) turbofan models to meet the UCAV's mission requirements. The minimum required thrust is 1490 lbf, with engine dimensions, weight, and specific fuel consumption (SFC) as critical factors. Among six candidates (Table 10), the Williams FJ33-5A was selected due to its higher power output, adaptability for future upgrades, and

comprehensive performance data. However, compatibility at high speeds (Mach 0.90 during dash) requires further verification. Despite this, the FJ33-5A's performance and data availability made it the optimal choice.

Table 10. Reviewed candidate LBR turbofan engines for the UCAV

Engine Model	Specifications					
	Length (in.)	Diameter (in.)	Max. Thrust (lbf)	Dry Weight (lb)	SFC (lb/lbf/hr)	Bypass Ratio
GE-Honda HF120 [24]	59.5	30.51	2095	466	< 0.7	2.9:1
PBS TJ200 [25]	27.74	9.68	512.5	61.73	–	–
PW615 [26]	49.5	30.0	1460	308.6	–	2.8:1
PW617 [27]	54.0	30.0	1891	379.2	–	2.7:1
Williams FJ33-5A [28]	47.9	24.75	1846	319	0.486	–
Jahesh-200 [29]	–	–	1543.2	459.3	~0.486	–

3. Wing Design

The UCAV's wing design is optimized for cruise-out efficiency, as this phase provides a consistent performance benchmark unaffected by payload jettison variability. Aerodynamic efficiency is achieved by minimizing drag while generating the ideal lift coefficient with acceptable moment characteristics. The average cruise-out mass, calculated from fuel fractions in Table 3, is:

$$W_{avg} = \frac{W_{cruise-out_initial} + W_{cruise-out_final}}{2} = 2227.69 \text{ lb}, \quad (22)$$

The ideal lift coefficient, derived from this mass and flight conditions, is adjusted by wing (0.95) and airfoil (0.855) correction factors to account for lift contributions from the fuselage, tail, and other components [21]. Similarly, the maximum lift coefficient at MTOW and sea level is computed and adjusted, with plain flaps tentatively selected as high-lift devices for their cost-effectiveness. The resulting key coefficients (Table 11) guide the wing design process: the ideal lift coefficient (C_{l_i}) ensures cruise efficiency, while the maximum ($C_{l_{max}}$) serves as a threshold for airfoil screening. Performance graphs and literature recommendations further refine the selection.

Table 11. Ideal lift coefficient at cruise and maximum required lift coefficient for the UCAV

Lift Coefficient	Mean Quantity			
	Cruise-out	Cruise-in	Dash-out	Dash-in
Aircraft ideal ($C_{L_{x,i}}$)	0.1111	0.0946	0.0670	0.0650
Wing ideal (C_{l_i})	0.1170	0.0995	0.0705	0.0684
Airfoil ideal (C_{l_i})	0.1300	0.1106	0.0784	0.0760
Aircraft Max. ($C_{L_{max}}$)			2.0000	
Wing Max. ($C_{L_{max,W}}$)			2.1053	
Airfoil Gross Max. ($C_{l_{max-gross}}$)			2.3392	
Lift-coefficient change due to HLD (ΔC_l)			0.8000	
Maximum lift coefficient ($C_{l_{max}}$)			1.5392	

3.1. Airfoil Selection

The airfoil selection process evaluated twenty candidate airfoils (all airfoil data were derived from [30,31]) based on their ability to meet the maximum required lift coefficient ($C_{l_{max}} = 1.5392$) and their

behavior at the ideal cruise lift coefficient. XFLR5 simulations (Figure 4) provided critical aerodynamic data, including drag coefficients (C_d), lift-to-drag ratios (C_l/C_d), and stall characteristics.

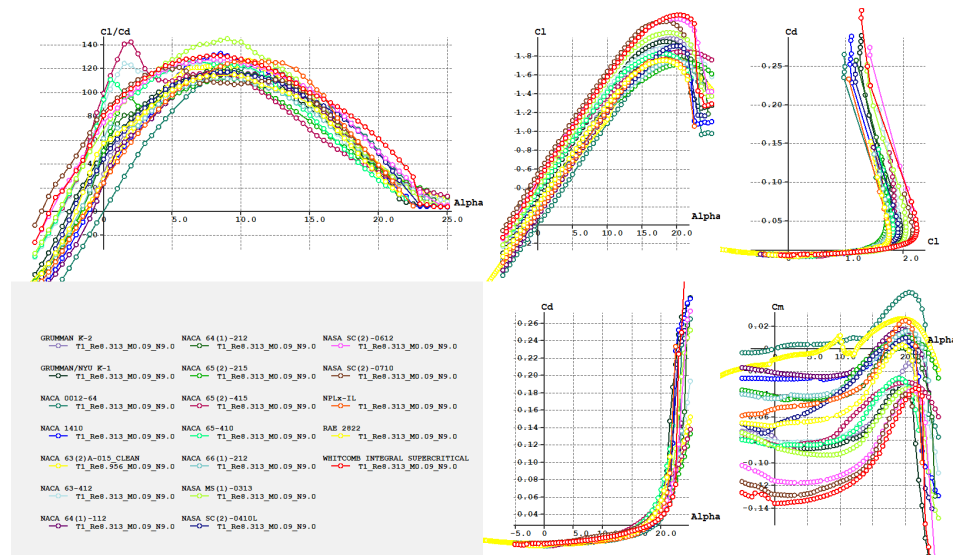


Figure 4. Aerodynamic properties of proposed airfoils in a cruise-simulated flow phase, produced in XFLR5 software

Initial screening rejected five airfoils for failing to meet the $C_{l_{max}}$ requirement. The remaining candidates were ranked by their drag coefficients at cruise conditions, with the seven highest-drag airfoils eliminated. A subsequent dash-phase analysis narrowed the pool to six candidates (Table 12). These were evaluated against four criteria:

- **Control:** Moment coefficients (C_m) near zero for agility and negative for stability.
- **Stall:** High stall angles to minimize stall speed.
- **Speed:** Low C_d for high-speed performance.
- **Endurance:** High C_l/C_d for efficient cruise.

Three airfoils were rejected during this phase: NACA 1410 due to excessive $C_{D_{min}}$ (0.00505), NASA SC₂ – 0410 for poor cruise efficiency with lowest C_L/C_D (116.73) and abrupt stall at 16° during the approach phase, and NACA 63-412 with lack of standout performance. The final candidates—NACA 65-410, NACA 63(2)A-015, and NACA 65(2)-415—underwent further testing in OpenVSP Software. NACA 65-410 offered balanced performance with a high stall angle, while NACA 63(2)A-015 featured favorable moment coefficients for high-speed control. NACA 65(2)-415 emerged as the most aerodynamically efficient, with the lowest $C_{d_{min}}$ and highest $(C_L/C_D)_{max}$.

Table 12. Prevailing candidate airfoils' aerodynamic performance produced by XFLR5 during cruise. The stall quality is described when simulated in the 'approach' conditions.

Airfoil	$C_{d_{min}}$	C_{m_0}	α_s	α_0	$(\frac{C_l}{C_d})_{max}$	C_{l_a}	Stall Quality
NACA 1410	0.00505	-0.0263	17.0°	-1.11°	132.32	6.34 rad ⁻¹	Moderate
NACA 63 ₂ (A) - 015	0.00448	-0.0143	16.0°	-1.30°	125.38	6.09 rad ⁻¹	Docile
NACA 63 - 412	0.00413	-0.0777	15.5°	-3.03°	123.99	6.33 rad ⁻¹	Docile
NACA 65 ₂ - 415	0.00361	-0.0785	17.0°	-3.09°	142.06	6.24 rad ⁻¹	Docile
NACA 65 - 410	0.00435	-0.0814	19.0°	-3.13°	127.03	6.17 rad ⁻¹	Docile
NASA SC ₂ - 0410	0.00497	-0.0726	16.0°	-2.14°	116.73	5.54 rad ⁻¹	Sharp

For OpenVSP testing using the VSP-Aero package, the airfoils became wings, all configured with a 37.3° leading-edge sweep (per [21]), a taper ratio of 0.25, and thickness-to-chord ratios of 0.11 (root) and 0.10 (tip). VSP-AERO uses a *vortex-lattice or panel solver aerodynamics method*, which does not take into account boundary layer effects. Simulations employed the panel method (17 sections, 64 wake nodes) to capture thickness effects, with vortex lattice method (VLM) used after control-surface integration due to software constraints.

Final candidates tested in OpenVSP/VSP-Aero:

- **NACA 65-410:** High stall angle and acceptable $(C_l/C_d)_{max}$.
- **NACA 63(2)A-015:** Despite having the highest $C_{d_{min}}$ of the remaining, it featured a favorable moment coefficient (C_{m_0}) for stability, but agility.
- **NACA 65(2)-415:** Optimal aerodynamic efficiency, with the lowest $C_{d_{min}}$ and highest $(C_l/C_d)_{max}$.

– Dash & Cruise Condition Testing

Initial dash testing in OpenVSP evaluated three wing candidates (NACA 65-410, 65(2)-415, and 63(2)A-015) for local sonic flow at Mach 0.90. Simulations at four angles of attack (aoa), corresponding to four conditions for each wing - C_{l_i} (0.07838), $C_{d_{min}}$, $(C_l/C_d)_{max}$, and an intermediate value - confirmed subsonic flow locally since the local velocity remained below the threshold of 1.111 or 1/0.9 (Figure 5). Subsequent analysis determined wing-specific aoas for achieving the ideal lift coefficient at dash ($C_{l_i} = 0.0705$) and cruise ($C_{l_i} = 0.1170$) (Table 13). These *aoas*, along with 0°, were used for aerodynamic comparisons, both in dash and in cruise conditions, in two analyses with identical methodology.

Table 13. The aoa where each wing produces the ideal lift coefficient C_{l_i} during dash and cruise

Wing	aoa at Dash ($C_{l_i} = 0.0705$)	aoa at Cruise ($C_{l_i} = 0.1170$)
NACA 65-410	-2.495°	-1.889°
NACA 65(2)-415	-2.401°	-1.729°
NACA 63(2)A-015	-0.223°	+0.477°

NACA 63(2)A-015 emerged as optimal, exhibiting:

- Near-zero negative moment coefficient for stability and maneuverability.
- Lowest aoa for ideal lift and minimal induced drag at 0° aoa
- Superior inverted flight capability due to the lowest induced drag and lift coefficient at 0° *aoa*, despite slightly higher induced drag than NACA 65-410.

It falls second to NACA 65-410 regarding the induced drag coefficient at C_{L_i} , however NACA 65-410 exhibits the worst moment coefficient, thus not being the prevailing candidate airfoil.

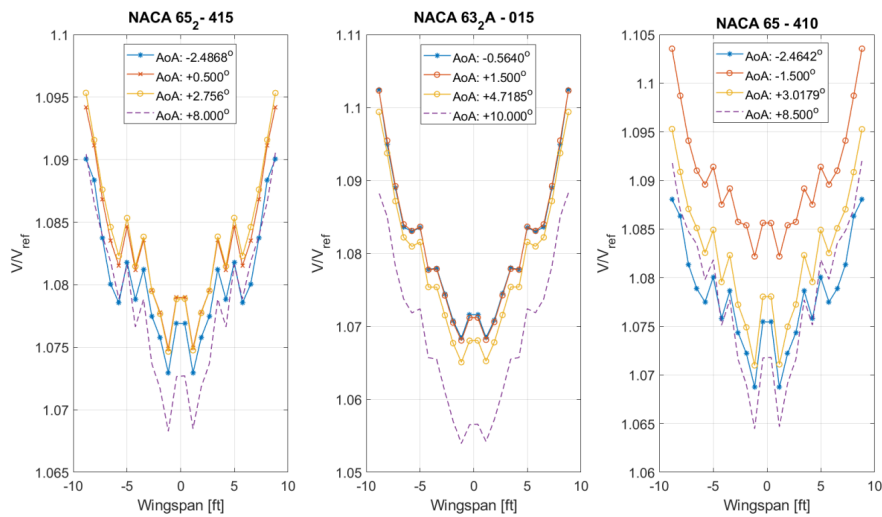


Figure 5. Local velocity versus reference (infinite) velocity around each airfoil during dash ($(t/c)_{\max_root}$: 11%, $(t/c)_{\max_tip}$: 10%)

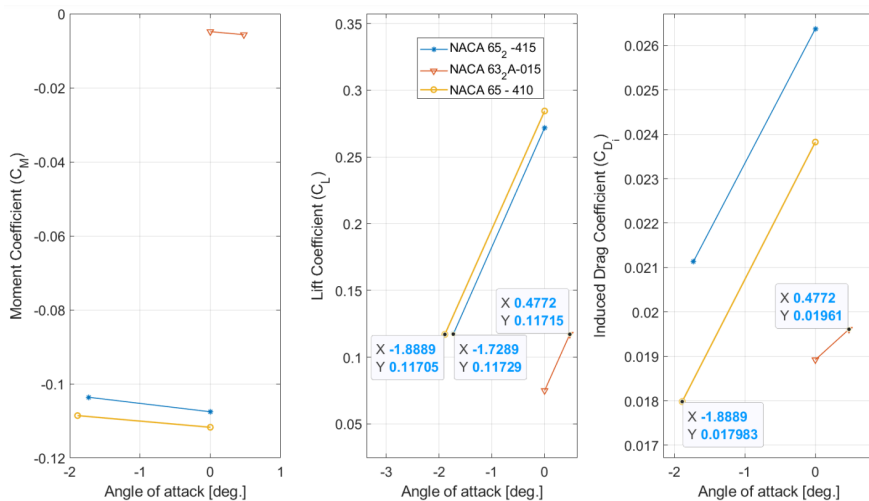


Figure 6. Moment, lift and drag coefficients as a function of aoa for the three candidate wings at cruise

3.2. Sweep, Taper and Thickness

Wing geometry optimization focused on preventing local sonic flow at Mach 0.90 while balancing aerodynamic/structural needs, particularly during dash phases where the aircraft flies at Mach 0.90 at 5000 ft. The analysis considers a range of angles of attack, from -5° to 20° , to assess performance across different flight conditions. The study evaluated:

- Taper ratios (λ): [0.20, 0.35, 0.60, 0.80]
- Sweep angles (Λ_{LE}): [35° , 37.3°]

OpenVSP simulations employed the Karman-Tsien compressibility correction [35], with lift distribution analyzed via normalized sectional coefficients ($C_l \cdot c / c_{ref}$). While more complex methods like the Prandtl-Glauert transformation [36] are typically used for 3D flows for moderate compressibility effects (still not valid in full transonic regimes), the Karman-Tsien correction provided sufficient accuracy for this analysis considering the available resources. Key findings:

1. Taper ratios 0.60/0.80 rejected due to positive moment coefficients (instability).
2. $\lambda = 0.35$ showed superior stall characteristics vs. $\lambda = 0.20$

3. 37.3° sweep marginally outperformed 35° with no sonic flow observed (Figure 5).

Lift distribution across the wingspan was analyzed using the sectional lift coefficient (C_l), normalized by the local chord length (c) and mean geometric chord (c_{ref}) as $C_l \cdot c/c_{ref}$. This metric correlates with load distribution, balancing the following objectives:

- Structurally, load should concentrate near the wing root to minimize bending moments.
- Aerodynamically, lift distribution should approximate an elliptical shape to reduce induced drag [20,21].

Even if the lift distribution itself is not perfectly elliptical, the combination of local lift and the local chord c can still yield an elliptical distribution if the wing's geometric parameters, such as taper ratio and sweep angle, are appropriately configured. Figures 7 and 8 present the results of the simulations.

In Figure 8, the three upper graphs present the sectional load distribution across the wing span, and the three lower graphs the sectional lift distribution. While the load distribution approaches the elliptical (desirable), it is obvious that the lift distribution deviates from it, more for some wing configurations than others. To validate the simulation results, theoretical methods including Lifting Line Theory (LLT) [21] were employed. While LLT provides reliable lift estimation within operational ranges (excluding stall effects), significant discrepancies emerged when compared to OpenVSP outputs.

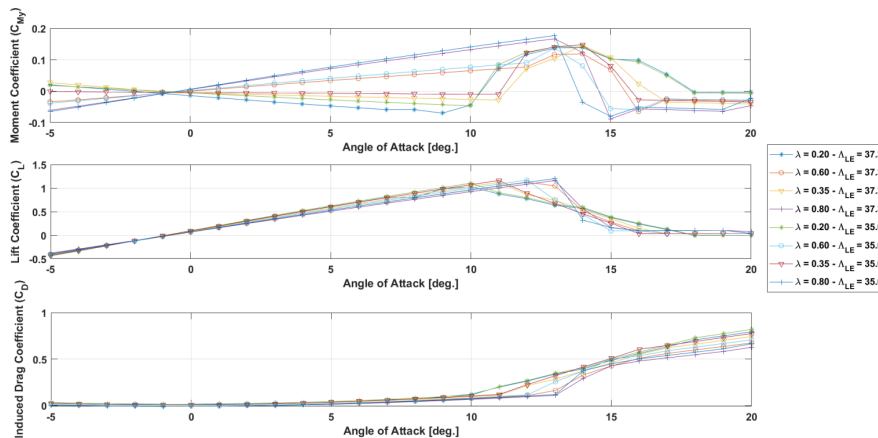


Figure 7. Comparison between lift, drag and moment coefficients for all 8 configurations of the wing at cruise

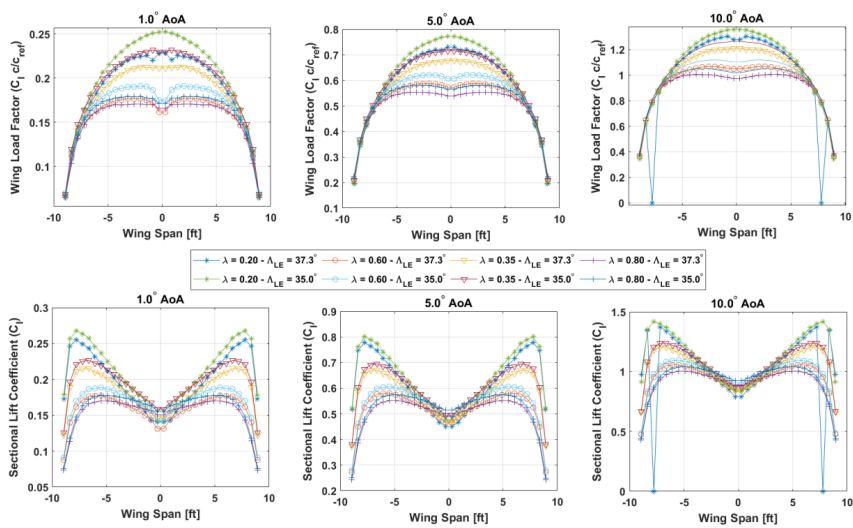


Figure 8. Wing load factor and sectional lift distribution for all wing configurations, cruise conditions in OpenVSP

These differences stem from LLT's linear assumptions failing to capture compressible flow effects at Mach 0.90, combined with potential limitations in VSP-Aero's drag prediction models [37].

Specifically, while LLT suggested a taper ratio of 0.22 would minimize induced drag ([2]), OpenVSP simulations consistently demonstrated superior performance with 0.35 taper ratio, exhibiting more favorable moment coefficients, higher stalling angles of attack, and marginally lower induced drag (Figure 9).

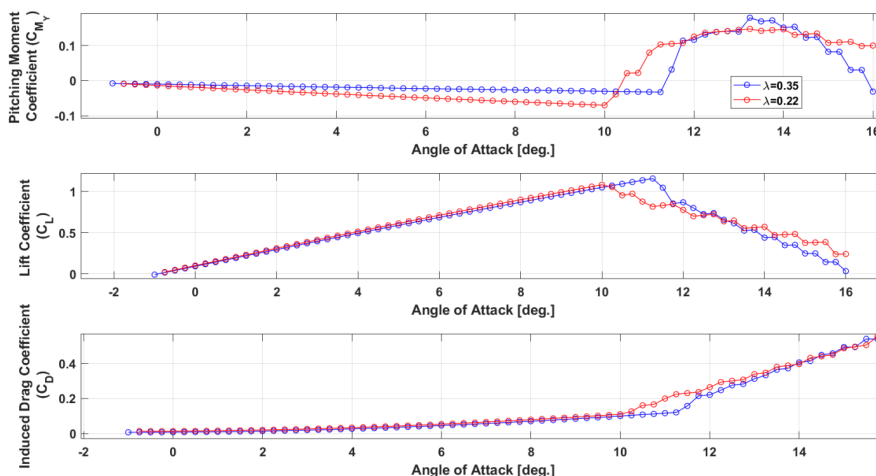


Figure 9. Wing moment, lift and induced drag coefficient comparison for two cases of taper ratio (twist angle: $i_w = 0.0^\circ$, $\Delta LE = 37.3^\circ$)

Given these inconsistencies and to maintain methodological consistency, the wing parameters were finalized based on OpenVSP results. This approach aligned with the design process methodology where airfoil and wing parameters were predominantly determined using computational tools (OpenVSP and XFLR5) as the primary reference. Further investigation and possibly the use of more sophisticated CFD tools may be required to reconcile these differences and achieve a more accurate assessment of induced drag for different taper ratios.

3.3. Wing Twist and Setting Angle

Wing twist is crucial for controlling the stall characteristics of the wing, ensuring that the wing root stalls before the tip. This is important because if the root stalls first, the ailerons, located near the wingtip, remain effective, allowing the pilot to maintain control of the aircraft during a stall. Simulations are run to determine whether it would be significantly beneficial for wing twist to be implemented to the design. Avoiding this modification would result in simpler manufacturing of the wing with lower cost.

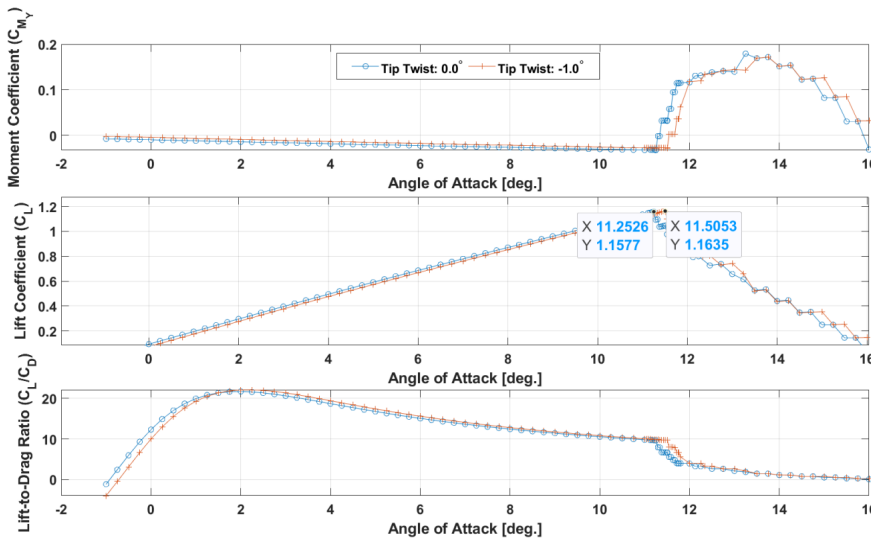


Figure 10. Wing moment, lift and induced drag coefficient comparison for two cases of tip twist ($\lambda = 0.35$, $\Lambda_{LE} = 37.3^\circ$)

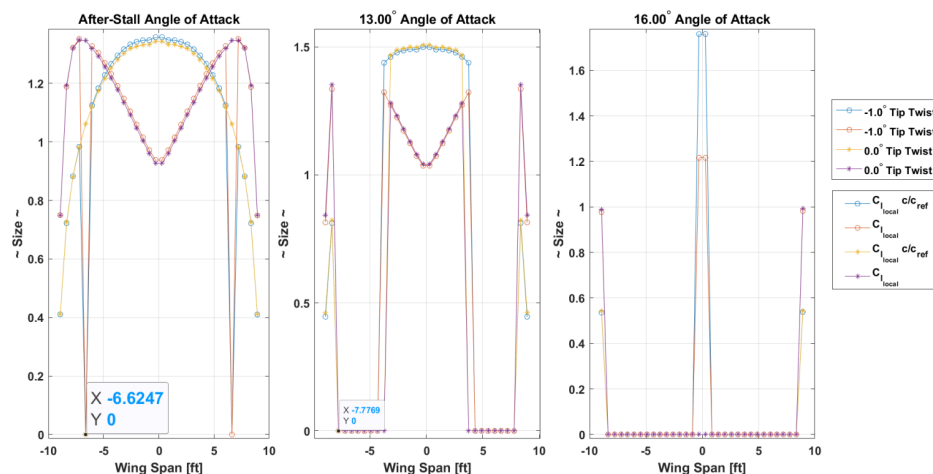


Figure 11. Load factor and sectional lift coefficient across the wingspan during stall for two cases of wing twist ($\lambda = 0.35$, $\Lambda_{LE} = 37.3^\circ$)

To evaluate the impact of wingtip twist on aerodynamic performance during cruise, two configurations were tested: one with 0.0° tip twist and another with -1.0° . Figure 10 compares the aerodynamic coefficients for both cases, revealing negligible differences, slightly favoring the -1.0° twist configuration. However, these differences are too minor to justify the added cost and complexity associated with manufacturing a twisted wingtip. Furthermore, Figure 11 illustrates the sectional wing loading factor and lift distribution at stall initiation, showing that stall does not originate at the wingtip. Since one of the primary purposes of tip twist is to mitigate tip-stall, its implementation is unnecessary in this design.

To further minimize the spread of stall across the wingspan, potential aerodynamic measures like wing fences could be explored. However, such interventions require detailed aerodynamic analysis and fall beyond the scope of this thesis. The wing setting angle, which ensures the optimal lift coefficient ($C_L = 0.1170$) during cruise, is determined through linear interpolation of the data in Figure 10 and given below:

$$\alpha_{\text{setting}} = +0.24^\circ \quad (23)$$

3.4. High-lift Devices (HLD)

To increase lift at lower speeds, the design initially uses plain trailing-edge flaps due to their simplicity and low cost. However, calculations based on [21,22] showed that even a 55° deflection angle—the typical limit for ensured structural integrity [22]—was insufficient for landing. To address this shortfall, the design process explored a compromise between achieving the required lift characteristics and adjusting the landing distance, since the *landing distance criterion* determines the wing area and is directly compromised by reducing the maximum lift coefficient ($C_{L_{max}}$) for landing without a complete wing redesign or adjustments to the required landing distance. Iterative analysis balanced these factors, allowing the adoption of a single-slotted flap configuration instead of more complex alternatives like Fowler flaps or leading-edge HLDs. This configuration offered an optimal trade-off between aerodynamic performance, structural simplicity, and cost.

The maximum lift coefficient's final value at landing is revised at 1.80, which suggests an increase of 33.35% for the total landing distance to 1333.35 feet. This pair of values allows for the wing reference surface to remain unchanged with a toll of 333.35 extra feet or 101.61 meters for the landing distance. For takeoff, $C_{L_{max}}$ was reduced to 1.50, lowering flap deflection and drag. Table 14 summarizes the finalized flap parameters, while Figure 12 depicts the top view, showing flaps, ailerons, and the aircraft's aerodynamic center (ac_{wf}), typically at 20-30% MAC [21].

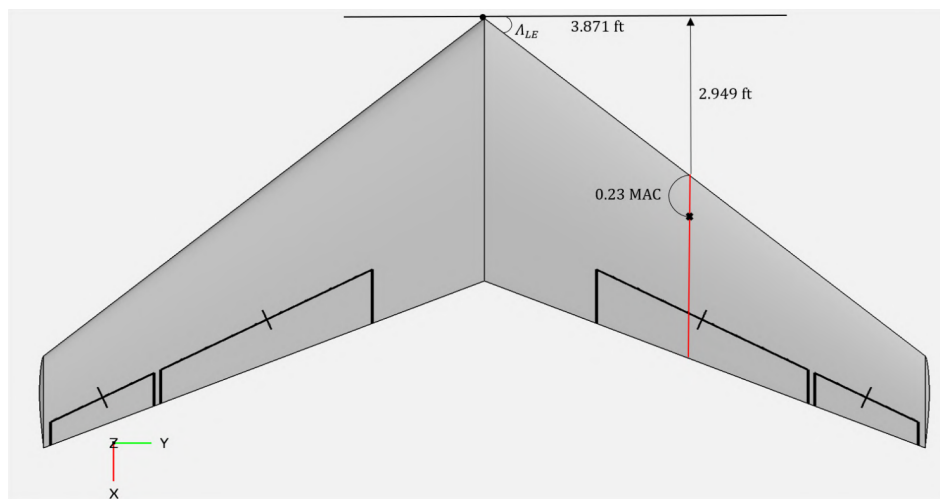


Figure 12. Wing top-view: Wing/fuselage aerodynamic center distances with respect to the wing geometry

3.5. Wing Weight

3.5.1. Wing Structure

The wing weight was estimated based on the methods presented by M. Sadraey [21] that account for gravity, material density, and load factors. The wing was designed with a maximum load factor of 6.5 (yields an ultimate design load factor of 9.75 based on typical values mainly for training fighter aircraft). A material density of 5.45 slugs/ft³ was determined based on an assumed composition of 55% aluminum, 35% CFRP, and 10% steel. The resulting wing constitutes 6% of the MTOW and that is for the wing structure only. Fuel, actuators, fuel tanks and systems are not included.

$$W_{\text{wing}} = S_{\text{ref}} \cdot \bar{C} \cdot \left[\frac{AR \cdot n_{\text{ult}}}{\cos(\Lambda_c/4)} \right]^{0.6} \left(\frac{t}{c} \right)_{\text{max}} \cdot \rho_{\text{wing}} \cdot K_p \cdot \lambda^{0.04} \cdot g = 145.5 \text{ lbs} \quad (24)$$

3.5.2. Fuel Capacity

The wing fuel capacity (V_{WF}) of the "Tísis" UCAV, in ft³, was estimated using the empirical formula from [22]:

$$V_{WF} = 0.54 \frac{S_{\text{ref}}^2}{b} \left(\frac{t}{c} \right)_{\text{root}} \frac{1 + \lambda \sqrt{\tau_w} + \lambda^2 \tau_w}{(1 + \lambda)^2} \quad (25)$$

where S_{ref} is the wing reference area (ft^2), b the wingspan (ft), $(t/c)_{root}$ the thickness-to-chord ratio, λ the taper ratio, and τ_w the ratio $(t/c)_{tip}/(t/c)_{root}$. The formula accounts for fuel storage up to approximately 85% of the span to avoid fuel near the tips, reducing fire risk from lightning strikes. Initially, (t/c) values of 0.11 (root) and 0.10 (tip) left a 70-liter shortfall. To correct this, the ratios were adjusted to 0.12 (root) and 0.11 (tip). VSP-Aero simulations confirmed the absence of sonic flow during critical phases (dash and cruise) with these refined values [2]. Using these updated parameters in Equation (25), the wing accommodated 0.3657 m^3 (12.92 ft^3) of fuel, still 40 liters short of the required 0.4049 m^3 (14.30 ft^3 , assuming a fuel density of 807.5 kg/m^3 [21]). The shortfall was covered by two small fuselage trim tanks. External tanks were avoided to preserve aerodynamic performance and minimize radar cross-section. Wing parameters are summarized in Table 14.

Table 14. Concentrated Main Wing Specifications

Wing Parameter	Nomenclature	Value
Aspect Ratio	AR	5.0
Leading Edge Sweep Angle	Λ_{LE}	37.3°
Quarter Chord Sweep Angle	$\Lambda_{c/4}$	33.6°
Taper Ratio	λ	0.35
Wing Span	b	18.444 ft
Mean Geometric Chord	C or c_{mgc}	3.689 ft
Mean Aerodynamic Chord	MAC	3.974 ft
Wing Reference Area	S_{ref}	68.039 ft ²
Root Chord	c_{root}	5.465 ft
Tip Chord	c_{tip}	1.913 ft
Max. Thickness-to-Chord Ratio (Root)	$(t/c)_{root}$	0.12
Max. Thickness-to-Chord Ratio (Tip)	$(t/c)_{tip}$	0.11
Airfoil Section	–	NACA 63 ₂ A-015
High-Lift Devices' Specifications		
Type	–	Single-slotted flaps
Flap-to-wing chord ratio	c_f/c	0.25
Span	b_{flap}	$(0.68-0.22) \cdot b/2$
Deflection at Takeoff	δ_{f_TO}	16°
Max. Deflection	$\delta_{f_{max}}$	40°

Now that all parameters are calculated, the wing's mean aerodynamic chord can be determined (Equation (27)) and the Oswald's coefficient e can be refined according to the following formula for swept wings [21]:

$$e = 4.61 \cdot (1 - 0.045 \cdot AR^{0.68}) (\cos \Lambda_{LE})^{0.15} - 3.1 = 0.76 \quad (26)$$

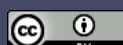
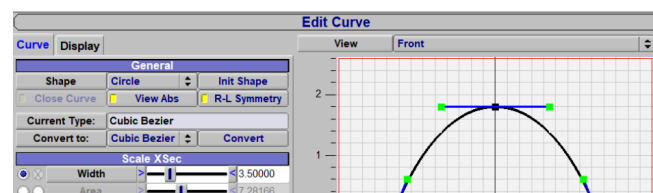
$$MAC = \frac{2}{3} c_{root} \left(\frac{1 + \lambda + \lambda^2}{1 + \lambda} \right) = 3.9739 \text{ ft} \quad (27)$$

The refined value for e is used to reassess the required thrust at 1457.58 lbf (previous value: 1483.95 lbf). Additionally, it is observed that the difference between MGC and MAC is 0.285 ft or 8 cm, a very small proportional difference which is enough to justify the use of the mean geometric chord for calculations until all parameters are determined and MAC can be calculated accurately.

4. Fuselage Design

The fuselage design of the "Tísis" UCAV is designed to prioritize an efficient internal layout and stability during flight. Initial length estimates of 26.0 feet, based on statistical data from Class-III UAVs and UCAVs (Figure A1) were refined to 22.5 feet after considering stability, tail effectiveness, and wetted-area reduction.

The fuselage is divided into two sections: the front houses electronics, sensors, radar, and front landing gear, while the



rear contains the engine, exhaust, stabilizers, and rear landing gear. The payload bay is integrated with wing and landing gear placement (Figure 14–blue box). The engine duct, positioned on the upper fuselage, enhances protection from ground fire and debris while utilizing the fuselage and wing for radar shadowing. The rear section features a bell-curve cross-section, tapering from 3.50 ft (horizontal) and 3.00 ft (vertical) at the engine inlet to 3.30 ft and 2.20 ft at the tail attachment point, forming a cone-like shape linked to the tail design (Section 5). The fuselage diameter was determined by balancing flap span, internal volume, and drag minimization. With the Williams FJ33-5A turbofan's diameter of 24.75 inches (Table 10) setting the minimum requirement, the horizontal dimension was finalized at 3.50 feet to optimize aerodynamic efficiency and internal space. Two chined edges, inspired by designs like the XQ-58 Valkyrie and MQ-28 Ghost Bat, enhance aerodynamics and reduce radar cross-section. The engine is mounted rearward and slightly upward, creating space for rear landing gear and fuel tanks. An S-duct intake and exhaust configuration is assumed to maintain thrust efficiency while providing protection.

4.1. Fuselage Weight

The weight of the fuselage is estimated using the empirical formula in Equation (28). The fuselage is assumed to be constructed primarily of aluminum (52%), with additional kevlar components (8%), CFRP (30%), and steel (10%). This material combination yields a fuselage density of 2766.22 kg/m^3 . The fuselage density factor (K_{ρ_f}), which accounts for variations in fuselage design and internal components, is chosen as 0.00235 based on typical values for UAVs [21]. An engine inlet parameter (K_{inlet}) of 1.25 is applied since the fuselage incorporates engine inlets. The ultimate load factor is the same as the one assumed in Subsection 3.5.1 and the equivalent diameter (D_{equ}) is 3.171 ft. The calculated weight represents 8.36% of the UCAV's MTOW.

$$W_{\text{fuselage}} = L_f \cdot D_{\text{max}_f}^2 \cdot \rho_{\text{fuselage}} \cdot K_{\rho_f} \cdot K_{\text{inlet}} \cdot g \cdot n_{\text{ult}}^{0.25} = 202.81 \text{ lbs} \quad (28)$$

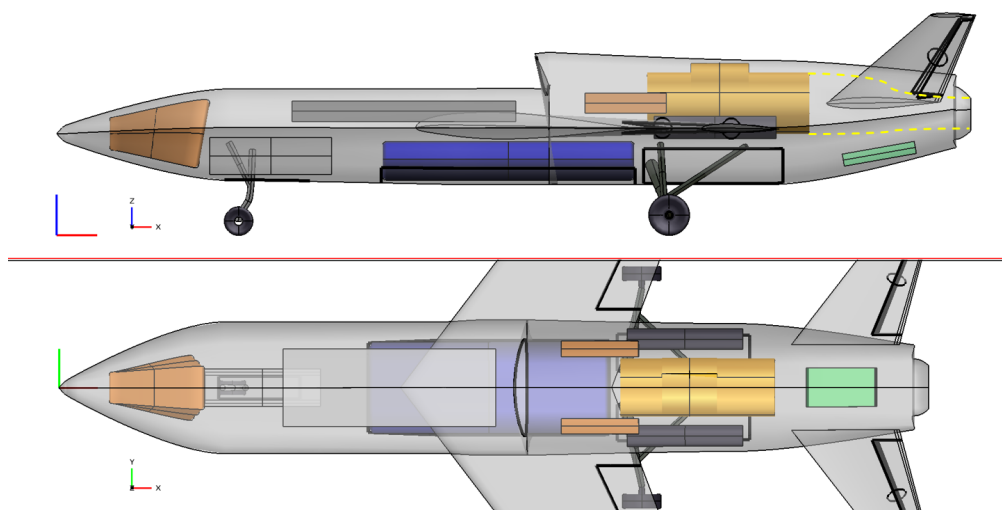


Figure 14. Transparent side-view and top-view of the UCAV highlighting the internal layout with landing gear extended.

5. Tail Design

5.1. Configuration and Initial Considerations

The initial design phase for the tail of the “Tísis” UCAV focuses on creating a conventional aft tail configuration. The goal is to establish a solid foundation for stability and control following the approach recommended by M. Sadraey [21], allowed for a systematic determination of key parameters, including the tail volume coefficients (\bar{V}_H and \bar{V}_V), planform areas, aspect ratios, airfoil selections, and incidence angles, all while considering the influence of factors such as wing downwash and fuselage shape. The design process emphasizes optimizing the tail for cruise conditions.

Aircraft like the “Tísis” UCAV are designed to be stable during flight but approach neutral stability to enhance maneuverability and agility. This ensures smaller control inputs result in quicker responses and also why most modern aircraft are very difficult to handle without fly-by-wire systems. Longitudinal stability requires the aerodynamic center (ac_{wf}) or neutral point to be located behind the center of gravity (cg) [22]. If the neutral point is ahead of the cg, disturbances can cause destabilizing moments, such as an uncontrollable pitch-up [21]. There are ways to move the center of gravity forward, by arranging the internal components differently. For now, the aircraft’s center of gravity is tentatively assumed to be at 55% of the fuselage length, across the longitudinal axis of the aircraft and placed 10 cm behind the aircraft’s neutral point. This arrangement ensures sufficient space for the tail, as the remaining fuselage length from the cg to the aft tip (10.13 ft) exceeds the optimal tail arm length ($l_{optimal}$) calculated in Equation (29).

5.2. Horizontal Tail

5.2.1. Tail Parameters

The tail design follows established conceptual design methodologies [21], prioritizing maneuverability and stability trade-offs typical of fighter aircraft. Key parameters are derived as follows:

- **Tail Moment Arm:** The optimal arm ($l_{optimal}$) is calculated (Eq. 29) to minimize drag while ensuring tail effectiveness, yielding **7.86 ft**. A correction factor ($K_c = 1.30$) accounts for fuselage end-shape effects and D_f symbolizes the fuselage’s equivalent diameter.

$$l_{optimal} = K_c \sqrt{\frac{4\bar{C} \cdot S_{ref} \cdot \bar{V}_H}{\pi \cdot D_f}} = 7.86 \text{ ft} \quad (29)$$

- **Tail Area:** The horizontal tail area (S_H) is determined via the tail volume coefficient ($\bar{V}_H = 0.40$), resulting in **12.78 ft²**:

$$S_H = \frac{\bar{C} \cdot S_{ref} \cdot \bar{V}_H}{l_{optimal}} = 12.78 \text{ ft}^2 \quad (30)$$

- **Pitching Moment:** The wing/fuselage pitching moment coefficient (C_{mo_wf}) is calculated (Eq. 31) using airfoil data from NACA 63(2)A-015 (wing) at cruise, yielding **-0.0047**:

$$C_{mo_wf} = C_{m_{af}} \frac{AR \cdot \cos^2 \Lambda_{LE}}{AR + 2 \cos \Lambda_{LE}} + 0.01 \alpha_t = -0.0047 \quad (31)$$

- **Aerodynamic Center:** The wing/fuselage aerodynamic center (ac_{wf}) is tentatively placed at **23% MAC** (Fig. 12), pending CFD validation in later studies.

Design Rationale:

- The \bar{V}_H value reflects fighter-like longitudinal instability for enhanced controllability.
- The $l_{optimal}/L_f$ ratio (**0.35**) slightly exceeds the typical **0.30** for aft-tailed designs due to engine integration constraints.

- Tail lift (Eq. 32) is derived from the trim equation, assuming 90% tail efficiency (η_H) for the V-tail configuration, which typically ranges between 85% and 95% for conventional aft tails [32]) :

$$C_{L_H} = \frac{C_{m_{o_wf}} + C_L(h - h_0)}{\eta_H \cdot \bar{V}_H} = -0.0387 \quad (32)$$

Aerodynamic Considerations:

- The tail is designed for cruise but sized to ensure low-speed stability (turning rates have not yet been taken under consideration).
- The process of airfoil selection is by now familiar to the reader being the same as the one followed in Subsection 3.1. Symmetric airfoil NACA 63A-010 is selected for its consistent performance at positive/negative angles of attack—long lift-curve slope ($C_{L_{\alpha_tail}} = 6.324$).
- The tail setting angle (-0.74°) accounts for downwash effects from the wing to the tail.

Stability: The static longitudinal stability derivative ($C_{m_{\alpha}} = -0.357$) is negative, confirming a stable design [21].

5.3. Vertical Tail

The process for designing the vertical stabilizer matches the one followed for the horizontal tail. The main objective of this design is to determine crucial parameters for the vertical stabilizer—its span, planform area and aspect ratio—to serve as an imaginary surface used as the V-tail's projection on the vertical axis. This approach is explained and depicted in Subsection 5.4. The aforementioned parameters are incorporated in the finalized V-Tail configuration.

5.4. V-Tail Adjustment

The designed conventional tail serves as the basis for the transformation into the final V-tail configuration, which replaces the traditional horizontal and vertical stabilizers with two angled surfaces and offers potential advantages for the "Tísis" UCAV. By reducing the number of surfaces, the V-tail promises a decrease in both weight and parasitic drag, crucial for efficiency during high-speed flight. In this study, the inherent challenges associated with V-tails, including their susceptibility to Dutch roll, adverse roll-yaw coupling, and the complexity of their control system are only mentioned.

The adjustment from a conventional to a V-tail starts with determining the point of attachment on the fuselage. The ideal location for the V-tail's root was chosen based on the fuselage cross-section where the tail would be mounted. The goal was to maximize the exposed surface area of the tail while ensuring that the entire root was enclosed within the fuselage for structural integrity. The specific dimensions and placement were dictated by the shape and size of the fuselage, with the tail's root carefully integrated into the contours of the aircraft.

The dihedral angle was determined through a geometric analysis, considering the projections of the originally designed horizontal and vertical tail surfaces. The final dihedral angle was chosen to ensure that the V-tail produced equivalent aerodynamic forces in both pitch and yaw axes, replicating the stability characteristics of the initial conventional tail design and validated from simulations conducted in VSP-Aero. The simulations focused on analyzing the airflow behavior around the V-tail during high-speed flight conditions, ensuring that the design remained within acceptable limits for local flow velocities. The setting angle and the rest of the parameters for the V-Tail are identical to the ones calculated for the horizontal tail of the UCAV, without taking into consideration the wing's downwash in cruising flight, since the V-tail is not influenced.

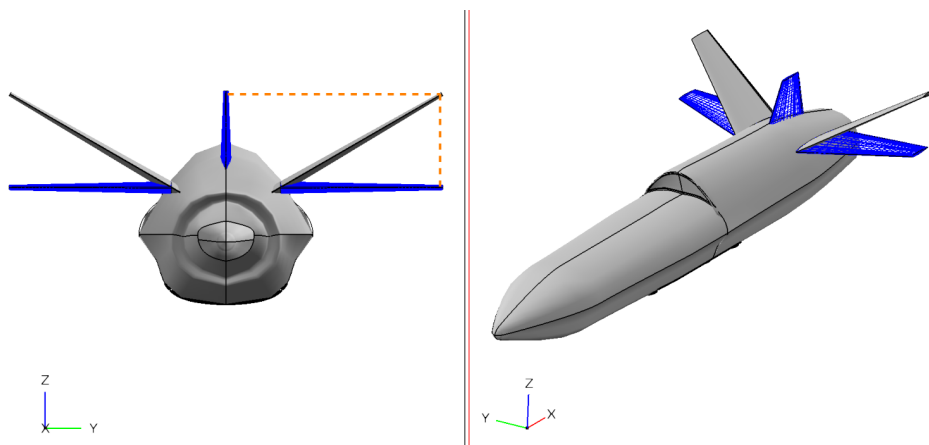


Figure 15. Adjustment from a conventional (blue tail) to a V-tail (gray tail) configuration in OpenVSP

5.5. Tail Weight

The tail weight estimation utilized a similar approach to the wing. A tail density factor (K_{ρ_T}) of 0.06 was selected based on data for fighter aircraft, acknowledging the tail's crucial role in stability and control during high-speed maneuvers. The material density was assumed to be the same as the wing, which is 5.45 slugs/ft³. The final tail weight is estimated at 15.11 lb representing 0.63% of the total MTOW.

Table 15. Concentrated V-Tail Specifications

Parameter	Nomenclature	Quantity
V-tail MGC	\bar{C}_{VT}	1.958 ft
V-tail MAC	MAC	2.078 ft
Tail span	b_{VT}	7.85 ft
Tail projection span	b_{projVT}	6.546 ft
Tail fin span	b_{fin}	3.925 ft
Root chord	C_{rootVT}	2.797 ft
Tip Chord	C_{tipVT}	1.118 ft
Taper ratio	λ_{VT}	0.40
Tail incidence	i_{VT}	-0.72°
Planform area	S_{VT}	15.37 ft ²
V-tail aspect ratio	AR_{VT}	2.79
Dihedral angle	Γ_{VT}	33.5°
Airfoil section	—	NACA 63A-010
V-tail sweep angle	Λ_{LE}	33.0°
Thickness-to-chord ratio	$(t/c)_{root}$	10%
	$(t/c)_{tip}$	9%
Tail type	—	Fixed or adjustable

6. Preliminary Stability Analysis

The main objective of this section is to confirm the assumptions made regarding the aircraft's cg during the tail design (Section 5). The study focuses on the theoretical stability analysis of the UCAV "Tisis," with practical flight testing and validation required for final confirmation of stability characteristics. The analysis aims to ensure that the center of mass follows a trajectory along the longitudinal axis of the UCAV that remains within close proximity to the initially estimated cg position, tentatively set at 55% of L_f .

6.1. Technical Details

The iterative process begins by placing each component inside the aircraft. The positions of the wing, the wing-stored fuel, the fuselage, and the tail are predefined relative to each other. The remaining components are positioned within the fuselage while considering the following assumptions:

- The **payload** (total available weight: 522.12 lb) is segmented into three sub-categories: 85% for the jettisoned payload (443.80 lb), 12% for additional subsystems (62.65 lb), and 3% for miscellaneous countermeasures (15.66 lb). The latter includes flare storage, with up to 19 MJU-7 A/B flares fitting within the allocated weight limit [38].
- The **landing system** weight is estimated based on empirical values for similar manned aircraft, as its precise design remains undetermined.
- The available weight for **standard equipment** is derived by deducting the other subsystems' estimated weight from MTOW.

Table 16 presents the final weight distribution and placement of each component as a percentage of MTOW. The trajectory of the *cg* throughout the mission profile, from ground loading to the final mission phase, is depicted in Figures 16 and 17. The *cg* is shown to shift between 53.02% and 56.17% of the fuselage's length (Case #1), maintaining a small and acceptable variation around the initially assumed 55% L_f .

To achieve stability, the aerodynamic center must remain aft of the center of mass. The following stability conditions were confirmed:

1. **Aerodynamic center** (ac_{wf}): Estimated at 23% of the wing's MAC, or 12.703 ft from the fuselage's nose (56.46% of L_f). This value is based on empirical data and requires validation through wind tunnel testing or CFD simulations.
2. **Center of gravity** (cg_{UCAV}): Ranges between 53.02% and 56.17% of L_f (11.93–12.64 ft).

Since both the upper and lower limits of cg_{UCAV} remain forward of ac_{wf} , the aircraft is deemed statically stable across all mission phases.

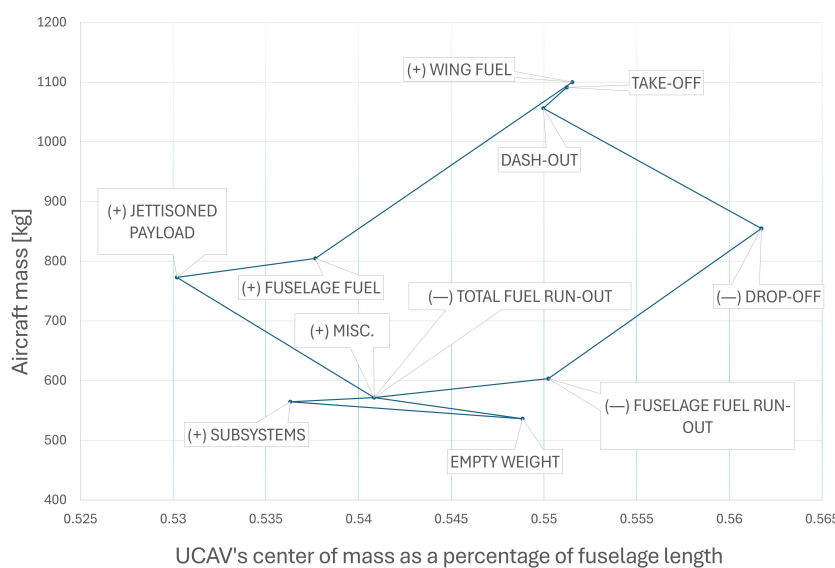


Figure 16. Center of mass movement along the longitudinal axis of the UCAV during all ground loading and flight phases—Case #1: Disposed Payload

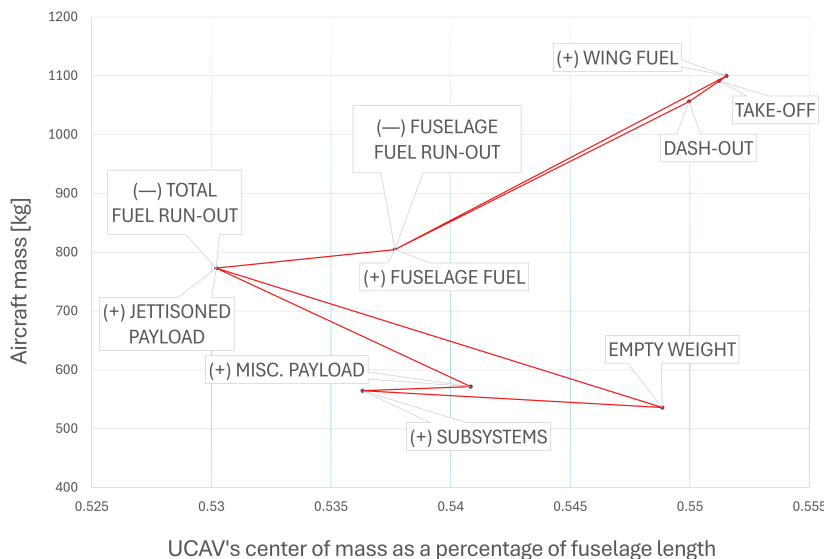


Figure 17. Center of mass movement along the longitudinal axis of the UCAV during all ground loading and flight phases—Case #2: Kept Payload

Table 16. Center of mass estimation for all individual components—Final Iteration.

UAV Component (<i>i</i>)	Weight		Relative Distance	
	Fraction (100% W_i/W_{TO})	Mass [lb]	from Reference Point	X_{cg_i} (%)
Engine	13.15%	319		72%
Fuel	Wing-stored	26.85%	651.13	58.93%
	Fuselage-stored	2.88%	69.74	72%
Payload	Subsystems	2.58%	62.65	30%
	Disposable	18.30%	443.80	50%
	Miscellaneous	0.65%	15.66	90%
Fuselage	8.36%	202.81		55%
Main Wing	6.00%	145.51		59.37%
Tail	0.63%	15.11		91.84%
Landing System	4.00%	97.00		55%
Standard Equipment	16.53%	400.93		38%

6.2. Methodology and Optimization Approach

The optimization method employed in this study follows a qualitative, iterative process rather than a formal algorithmic approach. The aircraft layout was refined manually using a spreadsheet-based method (Excel), where component placement was adjusted to satisfy aerodynamic, stability, and structural constraints. The optimization process followed these principles:

- The positions of the wing, wing-stored fuel, and tail were fixed relative to the fuselage based on aerodynamic and structural requirements.
- The **engine** was placed within the rear fuselage, aligning with the intake and outlet design constraints.
- Additional **fuel tanks** were positioned near the wing-stored fuel and engine to minimize the complexity and weight of the fuel distribution system.
- The **landing gear** placement followed empirical best practices, ensuring that the main landing gears were positioned aft of the *cg*, with a forward pivoting nose gear.

These constraints naturally shaped the layout of the UCAV, with component positioning iteratively refined until all functional and stability requirements were met. The design process was guided by engineering judgment rather than an automated optimization algorithm, ensuring that the final configuration adhered to practical and operational considerations.

7. Landing System

The UCAV features a retractable tricycle landing system with a single nose wheel and two main wheels positioned aft of the center of gravity. This configuration enhances directional stability, visibility, and crosswind handling while minimizing drag and radar cross-section. Geometric constraints, derived from literature [21,22], ensure safe clearances, including overturn, tipback, tailstrike, and wingstrike prevention angles, as detailed in Table 17.

Landing gear placement was determined iteratively through a trial-and-error process, considering the center of gravity and geometric restrictions. The nose gear is at 19.7% of the fuselage length, while the main gear is at 67%, 2.8 ft from the centerline. Wheel diameters are 7.8 inches (nose) and 10.2 inches (main), subject to future refinement. The main landing gear integrates two inclined struts and a jack, retracting within the fuselage without obstructing the rear wing spar or payload bay, while the nose gear comprises a single strut and jack. The final design of the landing system, while preliminary, represents a balanced approach that considers aerodynamic efficiency and structural feasibility.

Table 17. Landing system geometry restriction angles

Angle	Nomenclature	Calculated Value	Restriction
Overturn Angle	Φ_{ot_1}	45.86°	$\geq 25^\circ$
	Φ_{ot_1} (Stringiest)	54.96°	$\leq 55^\circ$
	Φ_{ot_2}	35.04°	$\geq 25^\circ$
Tip-back Angle	Φ_{tb_3}	41.87°	$\geq 15^\circ$
Tail-strike Angle	Φ_{ts_4}	16.14°	$\geq 15^\circ$
Wing-strike Angle	Φ_{ws_5}	22.42°	$\geq 5^\circ$

8. Final Design

Brief presentation of the landing system and the final conceptual sketch of the aircraft, as designed in [2]. The final design, though functional and kinematically sound, is qualitative at this stage. A more detailed design, including load analysis and precise component dimensions, would occur in a subsequent, detailed design phase that falls beyond the scope of this paper.

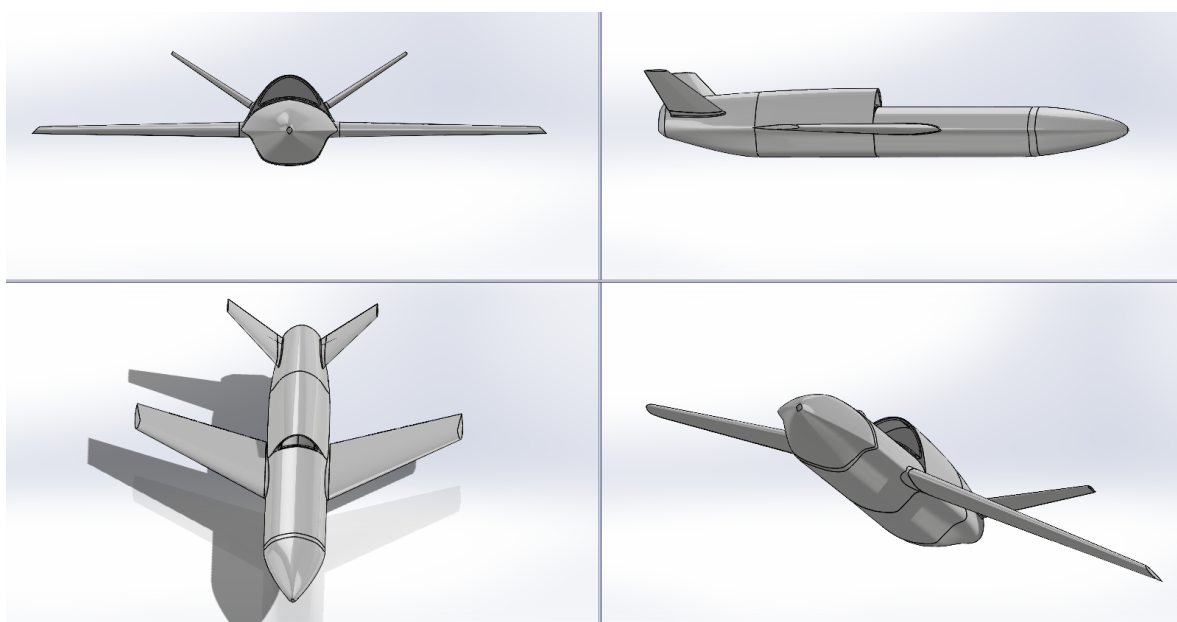
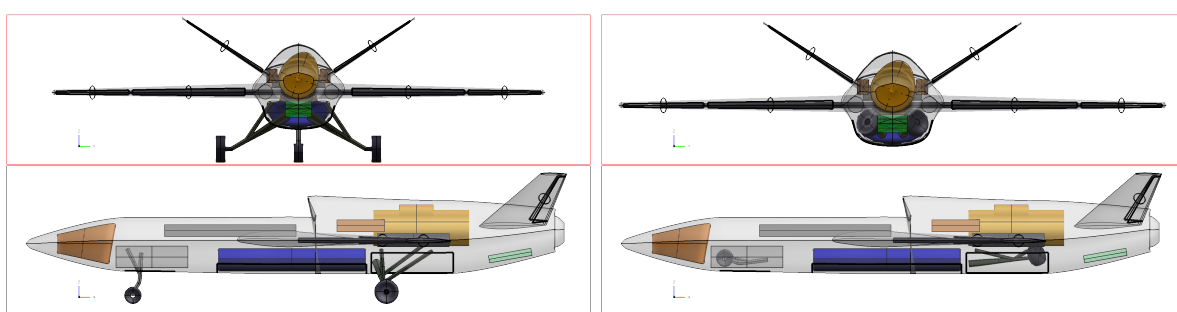


Figure 18. External image of the designed UCAV "Tisis" designed in SolidWorks.



(a) Landing gear extended

(b) Landing gear retracted

Figure 19. Left and rear view of the designed UCAV

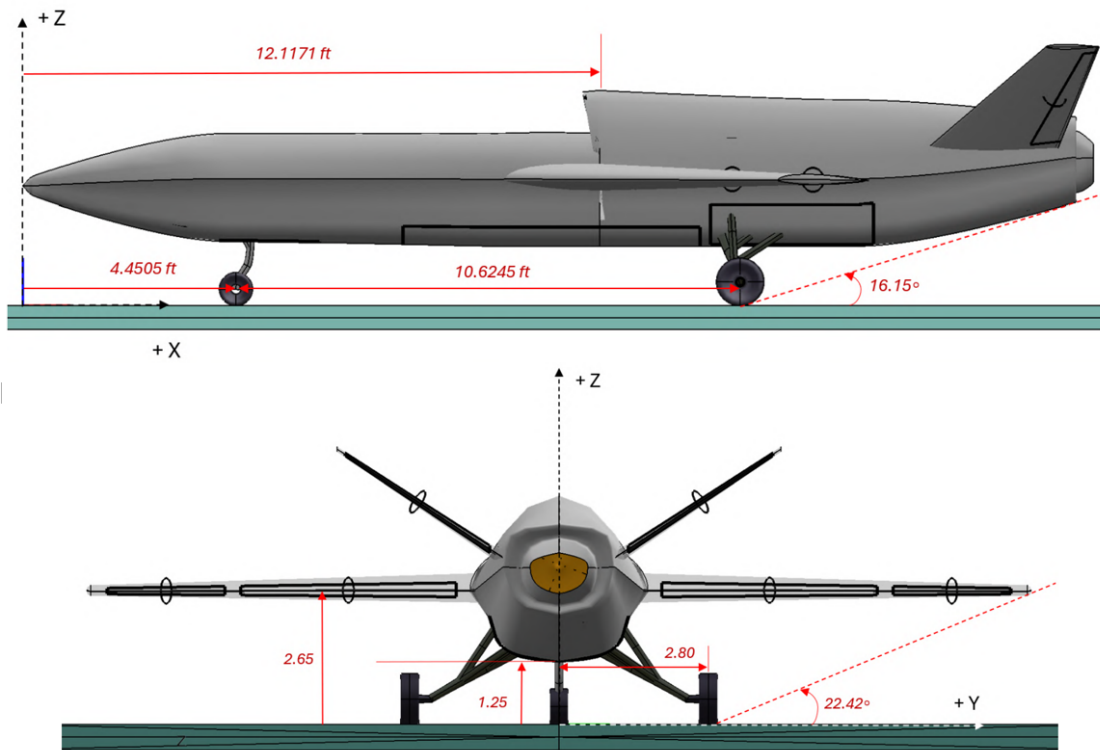


Figure 20. Left and rear view of the UCAV with dimensions.

Table 18. UCAV Specifications

Parameter	Quantity
Wing Configuration	Conventional
Wing Type	Fixed
High-lift Devices	Single-slot TE Flaps
Wing's geometrical specifications	<i>See Table 14</i>
HLD geometrical specifications	<i>See Table 14</i>
Tail Configuration	V-Tail
Tail's geometrical specifications	<i>See Table 15</i>
Fuselage Length (ft)	22.50
Fuselage Width (ft)	3.50
Landing System Configuration	Tricycle

8.1. Design Considerations for Further Improvement of the Concept

This section outlines potential enhancements to the UCAV's design. Stealth enhancements focus on reducing radar cross-section (RCS) and infrared signatures. Critical detectability sources include exposed engine fan blades, exhaust plumes, and sharp edges. Mitigation strategies adopt lessons from the XQ-58 Valkyrie (chined fuselage) and F-117 Nighthawk: enclosed bays for gear/payloads, an elevated engine duct, and a trapezoidal fuselage to scatter radar. Future work may integrate radar-absorbent materials or widened exhaust nozzles, pending detailed RCS analysis in subsequent studies.

Aerodynamically, achieving Mach 0.90 at 5,000 ft requires drag reduction and confirmed thrust adequacy. Current tools used (XFLR5, OpenVSP) lack transonic precision [37], but preliminary refinements on Tisis UCAV are underway [39]. Proposed improvements include F/A-18-style wing root extensions for flow separation control and wing fences to limit stall propagation. These features require tailored design and advanced CFD simulations for compatibility. Additionally, weight reduction efforts could target the traditional landing system, with gravity-based mechanisms replacing hydraulics. If applied, trolley-assisted takeoff (XQ-58 method [40]) could further simplify the design.

9. Discussion

The "Tísis" UCAV incorporates several design features aimed at minimizing drag and maximizing aerodynamic efficiency to achieve high-speed performance. Key design choices include:

- **V-Tail Configuration:** Reduces tail surface area and parasitic drag, beneficial for high-speed flight and potentially lowering RCS. Stability and control trade-offs are acknowledged.
- **Internal Payload Bays:** Minimize drag and RCS compared to external pylons.
- **Retractable Landing Gear:** Reduces drag during flight, despite added complexity and weight.
- **Fuselage Shaping:** A streamlined, compact fuselage with a top-mounted engine inlet minimizes drag and leverages the fuselage's shape to reduce RCS.
- **Wing Design:** Optimized sweep angle, taper ratio, and thickness-to-chord ratio to minimize drag, despite limitations in transonic flow modeling with current CFD tools.

The current design focuses on achieving a baseline configuration capable of fulfilling the mission profile while maintaining market competitiveness. Control surfaces are sized based on wing space and stability requirements, ensuring theoretical flight capability. Future refinements, such as optimizing roll and turn rates, can be addressed through additional control devices (e.g., spoilers) or alternative design changes (e.g., fully movable tail surfaces). These measures allow for flexibility in future improvements without requiring a complete redesign.

10. Conclusions

This study developed the conceptual design of the 'Tísis' UCAV to meet specific mission requirements using established aircraft design methods. The proposed configuration satisfies performance criteria, with future work focusing on technical maturation. Key recommendations include detailed aerodynamic analysis using high-fidelity CFD simulations for accurate transonic modeling near Mach 0.90, as current tools like XFLR5 and OpenVSP lack precision in these conditions [37]. Structural analysis must ensure airframe integrity under operational loads while optimizing critical components like the wingbox and exploring advanced materials.

Wing optimization should refine the planform, airfoil selection, and structural layout, including aeroelastic analyses. Subsequent phases involve detailed subsystem integration (avionics, propulsion, fuel systems) and prototype development for wind tunnel and flight testing. Finally, integrating advanced electronics and AI capabilities - including autonomous flight control, sensor fusion, and secure communications - will ensure operational reliability and interoperability with manned aircraft, enabling the 'Tísis' to achieve its intended performance goals—and attaching it to the profile of a Loyal Wingman.

Author Contributions: Conceptualization, Savvas Roussos and Vaios Lappas; Methodology, Eleftherios Karatzas; Software, Savvas Roussos; Supervision, Vassilios Kostopoulos and Vaios Lappas; Validation, Eleftherios Karatzas and Vaios Lappas; Writing – original draft, Savvas Roussos.

Funding: This research received no external funding

Conflicts of Interest: The authors declare no conflicts of interest.

Abbreviations

The following abbreviations are used in this manuscript:

AR	Aspect Ratio
CG	Center of Gravity
HLD	High Lift Device
LBL	Low Bypass Ratio
LLT	Lifting Line Theory
MAC	Mean Aerodynamic Chord
MGC	Mean Geometrical Chord
MTOW	Maximum Take-off Weight
RCS	Radar Cross Section
ROC	Rate of Climb
SFC	Specific Fuel Consumption
UCAV	Unmanned Combat Aerial Vehicle

Appendix A

Table A1. Air and flight characteristics in all altitudes of interest. (Data were calculated parametrically using Sunderland's method [41,42] and crosschecked through [43])

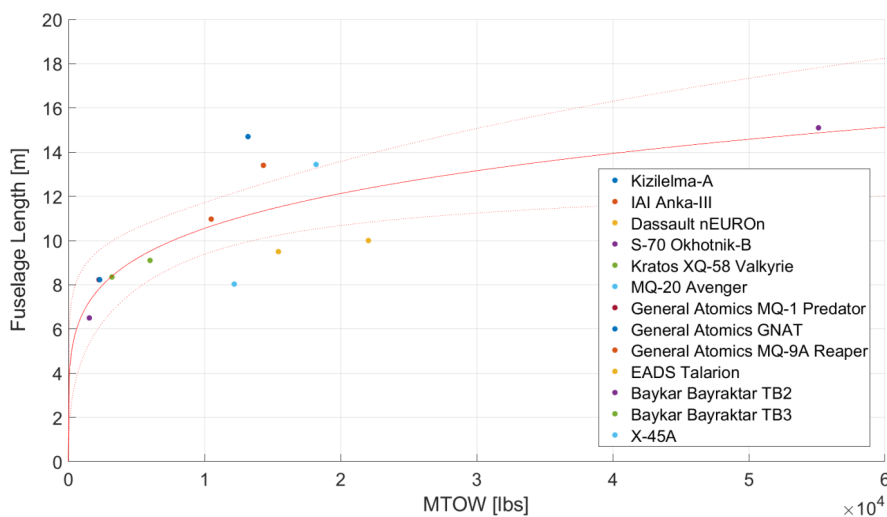
Parameter	Take-off & Approach	Cruise	Dash
Altitude [feet]	0	30000	5000
Temperature [K]	298.15	238.714	288.244
Air Pressure [kPa]	101325	84837.57	31493.43
Air Density [slugs/ft ³]	$22.9179 \cdot 10^{-4}$	$8.9178 \cdot 10^{-4}$	$19.895 \cdot 10^{-4}$
Dynamic Viscosity [kg/(m·s)]	$1.8371 \cdot 10^{-5}$	$1.5402 \cdot 10^{-5}$	$1.7898 \cdot 10^{-5}$
Sunderland's Constant (S)		110.4 K	
Ambient Temperature (Sealevel)		298.15 K	
Temperature Lapse Rate*** [K/m]		0.0065	
Specific Gas Constant [J/(kg·K)]		287.05	
Gravitational Acceleration [m/s ²]		9.80665	

** Calculated using the mean geometric chord as reference.

*** Valid up to 11 kilometers in altitude.

Table A2. Weight range of each component as a percentage of MTOW for various aircraft types [19].

Component	Aircraft Category				
	Civil Jets	Military Trainers	Fighters	Military Turboprop	Transport Turbofan/Turbojet
Structure	0.270-0.350	0.310-0.390	0.33-0.35	0.250-0.330	0.210-0.360
Propulsion System	0.065-0.075	0.140-0.190	0.20-0.30	0.070-0.110	0.050-0.080
Standard Equipment	0.090-0.130	0.150-0.180	0.12-0.18	0.060-0.100	0.040-0.070
Wing Assembly	0.090-0.140	0.070-0.110	0.13-0.17	0.070-0.130	0.090-0.130
Stabilizers	0.017-0.025	0.018-0.026	0.09-0.13	0.016-0.024	0.017-0.019
Fuselage	0.090-0.120	0.090-0.170	0.13-0.16	0.100-0.130	0.060-0.150
Landing System	0.038-0.045	0.040-0.070	0.04-0.06	0.035-0.045	0.035-0.050

**Figure A1.** Correlation between fuselage length and MTOW for various Class-III UAVs [2]

References

1. Castrillo, V.U., Manco, A., Pascarella, D. and Gigante, G., 2022. A review of counter-UAS technologies for cooperative defensive teams of drones. *Drones*, 6(3), p.65.
2. Roussos, S. Conceptual design of a turbofan – based Loyal Wingman UAV: Towards a Class – III aircraft. Master's Thesis. University of Patras, Patras, Greece, 2024.
3. Azman, K. The First Visuals of TAI ANKA-3 MIUS Have Been Shared! Defence Turk. December 2022. Available online: <https://www.defenceturk.net/tusas-anka-3-miusun-ilk-gorselleri-paylasildi> (accessed on 17 June 2024).
4. Kadidal, A. HAL Loyal Wingman Project to Go Airborne by 2024. Janes. Available online: <https://www.janes.com/osint-insights/defence-news/air/hal-loyal-wingman-project-to-go-airborne-by-2024> (accessed on 2 December 2024).
5. Baykar. Serial Production of Baykar's Drone Set to Begin in 2024. June 2023. Available online: <https://baykartech.com/en/press/serial-production-of-baykars-drone-set-to-begin-in-2024/> (accessed on 28 May 2024).

6. Waldron, G. Australian 'Loyal Wingman' to Form Basis of Boeing Skyborg Bid. FlightGlobal, 2021. Available online: <https://www.flighthglobal.com/defence/australian-loyal-wingman-to-form-basis-of-boeing-skyborg-bid/142239.article> (accessed on 13 July 2024).
7. Pittaway, N. Ghost Bat Program a Priority. The Australian, 2023. Archived on 25 May 2023.
8. The MQ-28A Ghost Bat, Unmanned Systems and the Future of Australian Air Power. YouTube. 2023. Available online: <https://www.youtube.com> (accessed on 10 August 2023).
9. Dassault Aviation. nEUROn. Available online: <https://www.dassault-aviation.com/en/defense/neuron/> (accessed on 21 August 2024).
10. Miller, D. MiG and Sukhoi to Join Forces on Russian UCAV. FlightGlobal, 2011. Available online: <https://www.flighthglobal.com/mig-and-sukhoi-to-join-forces-on-russian-ucav/101484.article> (accessed on 21 August 2024).
11. TASS. First Flight of Russia's Heavy Attack Drone Okhotnik Scheduled for 2019. TASS Defense, 2018. Available online: <https://tass.com/defense/1012351> (accessed on 21 August 2024).
12. Litovkin, N. First Photos Published of Russia's New Okhotnik Combat Drone. Russia Beyond the Headlines, 2019. Available online: <https://www.rbt.com/science-and-tech/329956-first-photos-published-of-russias> (accessed on 21 August 2024).
13. X-45 J-UCAV (Joint Unmanned Combat Air System). Available online: <https://www.airforce-technology.com/projects/x-45-ucav/> (accessed 16 December 2024).
14. X-45 Joint Unmanned Combat Air System. Archived on 23 March 2008. Available online: https://web.archive.org/web/20080323161907/http://www.boeing.com/history/boeing/x45_jucas.html
15. International Civil Aviation Organization. *Manual of the ICAO Standard Atmosphere (Extended to 80 Kilometers (262,500 Feet)*, 3rd ed.; Doc 7488-CD; International Civil Aviation Organization: Montreal, QC, Canada, 1993; ISBN 978-92-9194-004-2.
16. Rogoway, T. More Details On Kratos' Optionally Expendable Air Combat Drones Emerge. The Drive. 2017. Archived from the original on 9 June 2023. Available online: <https://www.thedrive.com/the-war-zone/7845/more-details-on-kratos-optionally-expendable-air-combat-drones-emerge> (accessed on 13 August 2024).
17. Liptak, A. 'Skyborg' Could Let F-35 and F-15 Fighter Jets Control Their Own Companion Drones. The Verge, 2019. Available online: <https://www.theverge.com/2019/5/22/18635935/skyborg-f35-f15-fighter-jets-control-companion-drones-air-force> (archived on 7 January 2024; accessed on 23 May 2019).
18. Mizokami, K. The Air Force's New Weapon Is...Shipping Containers? Popular Mechanics, 2020. Available online: <https://www.popularmechanics.com/military/a31171784/air-force-shipping-containers/> (archived on 8 November 2023; accessed on 6 May 2022).
19. Roskam, I. *Airplane Design. Part 1: Preliminary Sizing of Airplanes*; Revised: November 4, 2002; DARcorporation: Lawrence, KS, USA, 1985.
20. Raymer, D.P. *Aircraft Design: A Conceptual Approach*, 6th ed.; American Institute of Aeronautics and Astronautics, Inc.: Reston, VA, USA, 2018.
21. Sadraey, M.H. *Aircraft Design: A Systems Engineering Approach*; John Wiley & Sons: Hoboken, NJ, USA, 2012.
22. Kallinteris, I. *Aircraft Preliminary Design*. Class Notes, Mechanical Engineering and Aeronautics Department, University of Patras, 2023.
23. Jenkinson, L.R. and Marchman, J., Aircraft design projects: for engineering students. Elsevier, 2003.
24. Honda Motor Co., Ltd. Honda Aero Engine HF120. 2024. Available online: <https://global.honda/en/products/aeroengine/HF120.html> (accessed on 3 September 2024).
25. PBS Velká Bítěš. Jet Engine PBS TJ200. 2024. Available online: <https://www.pbs.cz/en/Products/Aerospace/Aircraft-Engines/Jet-engine-PBS-TJ200> (accessed on 3 September 2024).
26. Pratt & Whitney Canada Corp. TYPE-CERTIFICATE DATA SHEET for PW615 Series Engines. Technical Report IM.E.025, Issue 01. European Aviation Safety Agency (EASA), Longueuil, Quebec, Canada. March 2007. Available online: <https://www.easa.europa.eu/en/document-library/type-certificates/pw615> (accessed on 3 September 2024).
27. Pratt & Whitney Canada Corp. TYPE-CERTIFICATE DATA SHEET for PW617 Series Engines. Technical Report IM.E.125, Issue 02. European Aviation Safety Agency (EASA), Longueuil, Quebec, Canada. May 2017. Available online: <https://www.easa.europa.eu/en/document-library/type-certificates/pw617> (accessed on 3 September 2024).
28. Williams International. The Williams Fanjet Family. 2024. Available online: <https://www.williams-int.com/products/> (accessed on 3 September 2024).

29. Hyvor Talk. Iran's 1st Turbofan Engine: Jahesh-700. Iran Press, 28 May 2022. Available online: <https://iranpress.com/irans-1st-turbofan-engine-jahesh-700> (accessed on 10 September 2024).
30. Melin, T. Parametric Airfoil Catalog, Part II: Göttingen 673 to YS930—An Aerodynamic and Geometric Comparison Between Parametrized and Point Cloud Airfoils; 2013.
31. Airfoil Tools. Airfoil Database and Tools. Accessed: 14 June 2024. Available online: <http://airfoiltools.com> (accessed on 14 June 2024).
32. Katsamanis, Z. Conceptual design and construction of a small canister based deployable UAV from composite materials. Master's Thesis. University of Patras, Patras, Greece, 2024.
33. Gudmundsson, Snorri. General aviation aircraft design: Applied Methods and Procedures. Butterworth-Heinemann, 2013.
34. Department of Defense. Standard Practice MIL-STD-3013A. In *Glossary of Definitions, Ground Rules, and Mission Profiles to Define Air Vehicle Performance Capability*. Department of Defense, Sept. 2008. Approved for public release; distribution is unlimited. Superseding MIL-STD-3013, 14 February 2003.
35. Tsien, Hsue-Shen. "Two-dimensional subsonic flow of compressible fluids." *Journal of spacecraft and rockets* 40, no. 6 (2003): 983-991.
36. Liu, Tianshu. "Pressure-correction method for low-speed pressure-sensitive paint measurements." *AIAA journal* 41, no. 5 (2003): 906-911.
37. iforce2d. OpenVSP Tutorial Part 2 (Pitch Moment and L/D Analysis). YouTube Video, 2019. Available online: https://www.youtube.com/watch?v=your_video_id (accessed on 2 September 2024).
38. N.d. F-22A Beddown Environmental Assessment Elmendorf Air Force Base, Alaska. Technical Report; Approved for Public Release; Distribution Unlimited. 6326 Arctic Warrior Drive, Elmendorf AFB, AK 99506: 3 Civil Engineering Squadron, 3 CES/CC, Elmendorf AFB, Alaska, 2006. Available online: <https://apps.dtic.mil/sti/pdfs/ADA634353.pdf> (accessed on 10 September 2024).
39. Panagos, S. Numerical computational simulation of flow around an aircraft using OpenFoam. Master's Thesis. University of Patras, Patras, Greece, 2024.
40. Trevithick, J. XQ-58 Valkyrie Can Now Take Off From Runways Thanks to New Launch Trolley System. The War Zone, 2024. Available online: <https://www.twz.com/air/xq58a-valkyrie-can-now-take-off-from-runways> (accessed on 3 July 2024).
41. Antonios I. Zografas, William A. Martin, and J. Edward Sunderland. *Equations of properties as a function of temperature for seven fluids*. Computer Methods in Applied Mechanics and Engineering, 61(2): 177–187, 1987.
42. W. Sutherland. The viscosity of gases and molecular force. *Philosophical Magazine*, 36(5): 507–531, 1893.
43. The Engineering ToolBox. U.S. Standard Atmosphere vs. Altitude. Available online: https://www.engineeringtoolbox.com/standard-atmosphere-d_604.html (accessed on 10/05/2024).

Disclaimer/Publisher's Note: The statements, opinions and data contained in all publications are solely those of the individual author(s) and contributor(s) and not of MDPI and/or the editor(s). MDPI and/or the editor(s) disclaim responsibility for any injury to people or property resulting from any ideas, methods, instructions or products referred to in the content.